Human coronaviruses disassemble processing bodies

Mariel Kleer[1,2,3*], Rory P. Mulloy[1,2,3*], Carolyn-Ann Robinson[1,2,3], Maxwell Bui-Marinos[1,2,3], Elizabeth L. Castle[4], Arinjay Banerjee[5,6,7], Samira Mubareka[8,9], Karen Mossman[10,11] and Jennifer A. Corcoran[1,2,3 #]

[1]Microbiology, Immunology and Infectious Diseases Department, University of Calgary, Calgary, AB, Canada.
[2]Charbonneau Cancer Research Institute, University of Calgary, Calgary, AB, Canada.
[3]Snyder Institute for Chronic Diseases, University of Calgary, Calgary, AB, Canada.
[4]School of Biomedical Engineering, University of British Columbia, Vancouver, BC, Canada.
[5]Vaccine and Infectious Disease Organization, University of Saskatchewan; Saskatoon, SK, Canada
[6]Department of Veterinary Microbiology, Western College of Veterinary Medicine, University of Saskatchewan; Saskatoon, SK, Canada
[7]Department of Biology, University of Waterloo; Waterloo, ON, Canada
[8]Department of Laboratory Medicine and Pathobiology, University of Toronto, Toronto, ON, Canada
[9]Sunnybrook Research Institute, Toronto, ON, Canada
[10]Department of Medicine, Master University, Hamilton, ON, Canada
[11]Institute for Infectious Disease Research, McMaster University, Hamilton, ON, Canada

[*]Equal contribution
[#]Corresponding Author

Abstract

The *Coronaviridae* are a family of viruses with large RNA genomes. Seven coronaviruses (CoVs) have been shown to infect humans, including the recently emerged severe acute respiratory syndrome coronavirus 2 (SARS-CoV-2), the causative agent of coronavirus disease (COVID-19). The host response to CoV infection is complex and regulated, in part, by intracellular antiviral signaling pathways triggered in infected cells. Pathogenic CoVs can hijack these antiviral responses, reshaping the production of interferons and proinflammatory cytokines. Processing bodies (PBs) are membraneless ribonucleoprotein granules that mediate decay or translational suppression of cellular mRNAs; this is particularly relevant for proinflammatory cytokine mRNA which normally reside in PBs and are repressed. PBs or their components are believed to play important direct-acting antiviral roles, providing a compelling reason for their frequent disassembly by many viruses. Prior to this report, no information was known about how human CoVs impact PBs. Here, we show that three human CoVs, SARS-CoV-2 and the common cold CoVs, OC43 and 229E, induce PB loss. Moreover, we screened a SARS-CoV-2 gene library and identified that expression of the viral nucleocapsid (N) protein from SARS-CoV-2 was sufficient to mediate PB disassembly. N protein mediated PB loss correlated with elevated transcript levels of selected proinflammatory cytokines that would normally be repressed in PBs. Ectopic expression of the N proteins from four other human coronaviruses (OC43, MERS, 229E and NL63) did not cause PB disassembly, suggesting that this feature is unique to SARS-CoV-2 N protein. These data indicate that SARS-CoV-2 disassembles PBs during infection. As an unintended side effect, the disassembly of PBs may enhance levels of proinflammatory cytokine mRNAs which normally reside in PBs, thereby reshaping the subsequent immune response.

Introduction

Processing bodies (PBs) are membraneless ribonucleoprotein (RNP) granules found in the cytoplasm of all cells [1,2]. PBs control cellular gene expression because they either degrade or sequester cellular RNA transcripts, preventing their translation into protein. PBs contain many enzymes required for mRNA turnover, including those needed for decapping (Dcp2 and co-factors Dcp1a and Edc4/Hedls) and decay of the RNA body (5'-3' exonuclease Xrn1 and RNA helicase Rck/DDX6) and some components of the RNA-induced silencing complex [3,4]. Not all coding RNAs are regulated by PBs, but those that are typically encode potent regulatory molecules like growth factors, pro-inflammatory cytokines, and angiogenic factors. One group of protein-coding mRNAs commonly found in PBs bear destabilizing AU-rich elements (AREs) in their 3'-untranslated regions (3'-UTRs) and include most proinflammatory cytokine transcripts [5-7]. These RNAs shuttle to PBs by virtue of interactions between the AU-rich element and RNA-binding proteins (RBPs). Once localized to PBs, most RNA transcripts are unable to undergo translation, although in rare cases translation repression can be reversible [3,8-11]. We and others showed that the presence of PBs correlates with increased turnover/suppression of ARE-mRNAs [7,12-15]. Conversely, when PBs are lost, constitutive ARE-mRNA suppression is reversed, and ARE-mRNA transcripts and/or their translation products accumulate. Therefore, PB disassembly can be viewed as a switch that permits cells to rapidly respond and translate ARE-containing proinflammatory cytokine RNA into molecules such as IL-6, IL-8, IL-1β, and TNF [5]. PBs provide an extra layer of post-transcriptional control enabling the cell to fine tune the production of potent molecules like proinflammatory cytokines.

Although PBs are constitutive, they are also dynamic, changing in size and number in response to different stimuli or stressors. This dynamic disassembly/assembly is possible because PBs

85 behave as biomolecular condensates that form via liquid-liquid phase separation of proteins [16-
86 19]. PBs form via sequential multivalent RNA-protein interactions, with a small group of
87 proteins that contain regions of intrinsic disorder serving as the essential scaffold onto which
88 additional proteins or RNA can be recruited as the PB matures [9,16,20-24]. Despite the
89 recognition of PBs as dynamic entities, our understanding of the signals that induce PB
90 disassembly remains incomplete. We and others have shown that stressors which activate the
91 p38/MK2 MAP kinase pathway, as well as many virus infections elicit PB disassembly
92 [12,13,15,25,26]. Disassembly can occur by a direct interaction between a viral protein(s) and a
93 PB component that is subsequently re-localized to viral replication and transcription
94 compartments (vRTCs) [27-29] or cleaved by viral proteases [30-32]. Viruses can also cause PB
95 disassembly indirectly by activating p38/MK2 signaling [12,13,26].
96
97 There are numerous reports of viral gene products that trigger PB disassembly, yet corresponding
98 reports of viral gene products that stimulate PB formation are rare, suggesting that PBs possess
99 direct antiviral function and their disassembly may favour viral replication in ways that we do
100 not yet grasp [33,34]. Even though other RNPs, such as stress granules, have emerged as
101 important components of our antiviral defenses that contribute to sensing virus and triggering
102 innate immune responses, evidence to support a direct antiviral role for PBs is less well
103 established [34-37]. A direct-acting antiviral role has been defined for several PB-localized
104 enzymes that impede viral replication (e.g. APOBEC3G, MOV10). However, in these cases, the
105 mechanism of viral restriction was attributed to the enzymatic activity of the PB protein(s)
106 whereas its localization to PBs was not deemed as significant [28,29,31,38-45]. Nonetheless, the
107 disassembly of PBs by diverse viruses strongly suggests they negatively regulate virus

replication, though it does create the following paradox. The reason viruses disassemble PBs may be to limit their antiviral activity; however, because PBs also control turnover/suppression of many proinflammatory cytokine transcripts, their disruption by viruses contributes to high proinflammatory cytokine levels as an unintended consequence.

The family *Coronaviridae* includes seven viruses that infect humans, including the four circulating 'common cold' coronaviruses (CoVs), HCoV-OC43, HCoV-229E, HCoV-NL63, and HCoV-HKU1 and three highly pathogenic viruses that cause severe disease in humans: MERS-CoV, SARS-CoV, and the recently emerged SARS-CoV-2 [46-51]. Severe COVID-19 is characterized by aberrant proinflammatory cytokine production, endothelial cell (EC) dysfunction and multiple organ involvement [52-64]. Even with intense study, we do not yet appreciate precisely how SARS-CoV-2 infection causes severe COVID-19 in some patients and mild disease in others though a mismanaged or delayed IFN response and an overactive cytokine response is thought to underlie severe outcomes [65-70]. Despite some contrasting reports, [71-73], what is clear is that SARS-CoV-2 proteins use a multitude of mechanisms to outcompete cellular antiviral responses [68,74-85].

To determine if SARS-CoV-2 and other CoVs interact with PBs to alter the cellular antiviral response, we performed an analysis of PBs and PB-regulated cytokine mRNAs after CoV infection. Prior to this research, no published literature was available on human CoVs and PBs, and only two previous reports mentioned PB dynamics after CoV infection. Murine hepatitis virus (MHV) was reported to increase PBs at early infection times, while transmissible gastroenteritis coronavirus (TGEV) infected cells displayed complete PB loss by 16 hours post

131 infection [86,87]. Observations that SARS-CoV-2 infection induced elevated levels of many PB-
132 regulated cytokines, such as IL-6, IL-10, IL-1β and TNF [53,54,57,69,70] suggested that human
133 CoVs like SARS-CoV-2 may reshape the cellular innate immune response in part by targeting
134 PBs for disassembly. We now present the first evidence to show that three human CoVs,
135 including SARS-CoV-2 trigger PB disassembly during infection. By screening a SARS-CoV-2
136 gene library, we identified that the nucleocapsid (N) protein was sufficient for PB disassembly.
137 However, this feature is not common for all human coronavirus N proteins, as overexpression of
138 MERS-CoV-N, OC43-N, 229E-N and NL63-N was insufficient to induce PB loss. SARS-CoV-
139 2 N protein expression was also sufficient to increase levels of inflammatory transcripts known
140 to be elevated in SARS-CoV-2 infection: IL-6 and TNF. Taken together, these results show that
141 PBs are targeted for disassembly by human CoV infection, and that this phenotype may
142 contribute to reshaping cytokine responses to SARS-CoV-2 infection.

Results

Infection with human coronaviruses causes PB loss

Endothelial cells (ECs) have emerged as playing a significant role in severe COVID; as sentinel immune cells they are important sources for many of the cytokines elevated in severe disease and are infected by SARS-CoV-2 *in vivo* [56,58-60,88]. However, others have shown that commercial primary human umbilical vein endothelial cells (HUVECs) require ectopic expression of the viral receptor, ACE2, to be susceptible to SARS-CoV-2 [89]. We recapitulated those findings and showed that after HUVECs were transduced with an ACE2-expressing lentivirus ($HUVEC^{ACE2}$), they were permissive for SARS-CoV-2 (Fig 1A). To use $HUVEC^{ACE2}$ for studies on PB dynamics, we confirmed that ACE2 ectopic expression had no effect on PB number in HUVECs (Fig S1). Confirming this, we infected $HUVEC^{ACE2}$ with SARS-CoV-2 to determine if PBs were altered. SARS-CoV-2 infected cells were identified by immunostaining for the viral nucleocapsid (N) while PBs were identified by immunostaining for two different PB resident proteins, the RNA helicase DDX6, and the decapping cofactor, Hedls. PBs, measured by staining for both markers, were absent in most SARS-CoV-2 infected $HUVECs^{ACE2}$ by 24 hours post infection (Fig 1B-E). We quantified the loss of cytoplasmic puncta using a method described previously [90] and showed that by 24 hours post infection, SARS-CoV-2 infected cells displayed a significant reduction in PBs compared to mock-infected controls (Fig 1C, E).

To confirm that PBs were reduced by SARS-CoV-2 infection of naturally permissive cells derived from respiratory epithelium, we infected Calu-3 cells with SARS-CoV-2. Infected cells were identified by immunostaining for N protein 48 hours after infection and PBs were stained for DDX6. We observed PB loss in most but not all infected cells (Fig 1F). PB loss was more

166 often associated with cells that displayed N-positive staining throughout the cytoplasm or N-
167 positive multinucleated syncytial cells and was less frequent in cells that had not yet fused or
168 displayed punctate N protein staining (Fig 1F). Our attempts to quantify PB loss in infected
169 Calu-3 were not successful because cell clumping and crowding displayed by these cells made it
170 difficult for our CellProfiler pipeline to identify discrete infected cells.
171
172 To determine if PBs were lost in response to infection with other human coronaviruses, we
173 established infection models for the *Betacoronavirus*, OC43, and the *Alphacoronavirus*, 229E.
174 We found HUVECs were permissive to both OC43 and 229E (Fig 2A-B). We then performed a
175 time-course experiment wherein OC43-infected HUVECs were fixed at various times post
176 infection and immunostained for the viral N protein and the PB-resident protein DDX6. We
177 observed that PBs were largely absent in OC43 N protein-positive cells but present in mock-
178 infected control cells (Fig 2C-D). 229E-infected HUVECs were stained for DDX6 to measure
179 PBs and for dsRNA to denote infected cells due to a lack of commercially available antibodies
180 for 229E. CoV infected cells are known to form an abundance of dsRNA due to viral replication
181 and transcription from a positive-sense RNA genome making this a suitable marker for viral
182 infection [91]. After 229E infection, we also found that PBs were significantly reduced (Fig 2D-
183 E).
184
185 PBs will disassemble if key scaffolding proteins are lost; these include the RNA helicase DDX6,
186 the translation suppressor 4E-T, the decapping cofactors Hedls/EDC4 and DCP1A, and the
187 scaffolding molecule Lsm14A [92]. To elucidate if CoV-infected cells displayed decreased
188 steady-state levels of PB resident proteins, we immunoblotted infected cell lysates for PB

proteins XRN1, DCP1A, or DDX6, and Hedls (Fig 3). SARS-CoV-2 infection of HUVEC^{ACE2} cells did not alter steady-state protein levels of these proteins compared to uninfected cells (Fig 3A). OC43-infected HUVECs displayed comparable levels of XRN1, DCP1A, and Hedls relative to uninfected cells; however, OC43 infection decreased steady-state levels of DDX6 at both 12 and 24 hpi (Fig 3B). 229E-infected HUVECs showed no detectible change in PB protein expression after infection compared to controls (Fig 3C).

PBs are important sites for the post-transcriptional control of inflammatory cytokine transcripts containing AU-rich elements, and PB loss correlates with enhanced levels of some of these transcripts [7,12-15]. To determine if ARE-mRNAs are elevated, and therefore subject to regulation during CoV infection, we harvested total RNA from SARS-CoV-2-, OC43- or 229E-infected HUVECs and performed RT-qPCR for five ARE-containing cytokine transcripts, IL-6, CXCL8, COX-2, GM-CSF, and IL-1β (Fig 4A-C). We observed increased levels of three of these transcripts, IL-6, CXCL8, and COX-2, compared to uninfected cells, particularly in SARS-CoV-2 infected cells (Fig 4A). Taken together, these data indicate that infection with human coronaviruses including SARS-CoV-2 induces PB loss, and that some PB-regulated cytokine ARE-mRNAs are elevated during CoV infection.

A screen of SARS-CoV-2 genes reveals mediators of PB loss

The genome of SARS-CoV-2 is predicted to contain up to 14 open reading frames (ORFs). The two N-terminal ORFs (1a and 1ab) encode two large polyproteins which are processed by viral proteases into 16 non-structural proteins (nsp1-16) essential for viral genome replication and transcription [46]. The 3’ end of the SARS-CoV-2 genome is predicted to code for ORFs that are

212 expressed from 9 subgenomic mRNAs [93]. Among these are the four structural proteins spike
213 (S), envelope (E), membrane (M) and nucleocapsid (N) and up to 9 potential accessory proteins,
214 not all of which have been validated as expressed in infected cells [93]. To test which SARS-
215 CoV-2 gene product(s) was responsible for PB disassembly, we obtained a plasmid library of 27
216 SARS-CoV-2 genes from the Krogan lab; this library included 14 nsps (excluding nsp3 and
217 nsp16), all structural (S, E, M, N) and candidate accessory genes (ORFs 3a, 3b, 6, 7a, 7b, 8, 9b,
218 9c, 10) [93]. We individually transfected each plasmid and immunostained for each of the
219 SARS-CoV-2 proteins using antibodies to the Strep-tag II and for PBs using anti-DDX6 (Fig
220 5A). Relative to control cells, many SARS-CoV-2 ORF transfected cells still displayed DDX6-
221 positive PBs; however, expression of some SARS-CoV-2 genes reduced DDX6-positive puncta,
222 including N and ORF7b (Fig 5A). We quantified the number of DDX6-positive PBs per cell for
223 each transfection as in [90] and found that the average number of PBs per cell was reduced
224 relative to our negative control after transfection of eight SARS-CoV-2 genes: nsp7, ORF7b, N,
225 ORF9b, ORF3b, nsp6, nsp1, and nsp11 (Fig 5B-C). This quantification was performed in two
226 different ways. In most cases, transfected cells were identified by co-staining for the Strep-tag II
227 fused to each gene, as shown for N, E and ORF7b (Fig 5A). In such cases, we quantified DDX6-
228 positive puncta only in those cells that were transfected and not in bystander cells (Fig 5B,
229 thresholded). These data identified three SARS-CoV-2 proteins that may cause PB loss in a cell
230 autonomous manner: nsp7, ORF7b and N (Fig 5B). For the remaining transfections (nsp1, nsp5,
231 nsp6, nsp11, nsp13, nsp14, ORF3b, ORF6, ORF9b, ORF9c) immunostaining for the Strep-tag II
232 was not robust and we were unable to threshold our PB counts. In these samples, we quantified
233 PBs in all cells of the monolayer (Fig 5C, unthresholded). These data identified five additional
234 SARS-CoV-2 proteins from our screen that may cause PB loss: ORF9b, ORF3b, nsp1, nsp6 and

nsp11 (Fig 5C). We verified the expression of all constructs, including low expressors (nsp1, nsp5, nsp6, nsp11, nsp13, nsp14, ORF3b, ORF6, ORF9b and ORF9c) by immunoblotting whole cell lysates harvested from parallel transfections (Fig 5D). We were unable to detect nsp4 by immunoblotting; however, we did visualize this protein by immunostaining (Fig 5D). We eliminated low confidence hits (nsp7, ORF9b) and low expressors (nsp6, nsp11) from further studies and proceeded with validation of the top four hits (ORF7b, N, ORF3b, nsp1).

The nucleocapsid protein of SARS-CoV-2 induces PB disassembly

We tested four top hits from our PB screen in more relevant endothelial cells as these cells can be infected, express inflammatory cytokines, and stain robustly for PBs. HUVECs were transduced with recombinant lentiviruses expressing N, nsp1, ORF3b, and ORF7b or empty vector control lentiviruses. We also included recombinant lentiviruses expressing nsp14 in this experiment because of its exoribonuclease activity and ability to diminish cellular translation and interferon responses [84]. Transduced cells were selected for transgene expression and then fixed and stained for the endogenous PB marker protein DDX6 and for the Strep-tag II on each of SARS-CoV-2 constructs. We observed robust staining of the viral nucleocapsid (N) protein in the transduced cell population (Fig 6A) but were unable to detect expression of nsp1, nsp14, ORF3b or ORF7b by immunostaining (Fig S2A). We quantified PB loss in the selected cells and observed decreased PB numbers in cell populations expressing N, nsp1, nsp14, ORF3b and ORF7b; however, the most robust PB loss was induced in N-expressing cells, which displayed a five-fold reduction in PB numbers as well as strong immunostaining (Fig 6B, Fig S2). We were concerned that we could not detect the other four transgenes by immunostaining; therefore, we performed immunoblotting for the Strep-II tag on lysates from each transduced cell population

(Fig S2C). Although we detected a strong band of ~50 kDa at the predicted molecular weight for N, we were unable to detect bands for nsp14, ORF3b and ORF7b, while the most prominent band for nsp1 did not migrate at the predicted molecular weight of ~20 kDa (Fig S2) [94,95]. For these reasons, we decided to focus the remainder of our analysis on the N protein.

As PBs are dynamic RNP granules that undergo transient disassembly and assembly, we wanted to determine whether N-mediated PB loss was caused by enhanced disassembly of PBs or the prevention of their *de novo* assembly. To determine this, we treated N-expressing HUVECs with sodium arsenite, a known inducer of PB assembly. Consistent with our previous observation, PB loss was observed post N expression in our untreated control (Fig 6C-F). However, in N-expressing cells that were treated with sodium arsenite, robust PB expression was still observed (Fig 6C-F). PBs were immunostained using two different PB resident proteins, DDX6 and Hedls. These data showed that N expression is sufficient to cause PB loss, and that the absence of PBs in N-expressing cells is a result of enhanced PB disassembly.

We showed that human CoVs OC43 and 229E also cause PB loss during infection (Fig 2); therefore, we were interested to determine if ectopic expression of nucleocapsid proteins from these or other human CoVs were sufficient to mediate PB disassembly. To test this, we transduced HUVECs with recombinant lentiviruses expressing the N protein from SARS-CoV-2 as well as N derived from two other Betacoronaviruses, MERS-CoV N-Flag and OC43 N. Expression of MERS-CoV and OC43 N proteins did not lead to significant PB loss compared to SARS-CoV-2-N (Fig 7A-B). We also tested two N proteins from human Alphacoronaviruses, 229E N-Flag and NL63 N-Flag and found that neither of these induced significant PB loss

compared to SARS-CoV-2 N (Fig 7C-D). Consistent with this, immunoblotting of steady state levels of PB resident proteins after N protein overexpression showed that most PB proteins tested remained unchanged in the context of ectopic expression (Fig 7E-F). The exception to this was the decapping factor, Hedls/EDC4, which was slightly decreased after expression of SARS-CoV-2 N, but slightly increased after expression of the four other N genes tested (Fig 7E-F). The significance of this observation is not yet clear.

To understand if PB disassembly correlated with changes to PB-regulated inflammatory cytokine transcripts, we performed RT-qPCR for the three AU-rich containing mRNAs, IL-6, CXCL8 and TNF that were elevated after infection with SARS-CoV-2, OC43 and 229E (Fig 4). PBs control cytokine transcript levels post-transcriptionally because they modulate mRNA decay; however, in uninduced ECs, the transcription of these mRNAs is minimal. For example, TNF mRNA could not be readily detected by RT-qPCR without transcriptional activation. Therefore, we treated control and N-expressing HUVECs with TNF to activate cytokine transcription and then assessed if N protein expression enhanced cytokine mRNA level post-transcriptionally. In the absence of TNF, no significant change of mRNA abundance was observed for any of the coronaviruses N proteins tested (Fig 8A-C, 0 hour no treatment). Ectopic expression of SARS-CoV-2-N enhanced transcript levels of IL-6, CXCL8, and TNF 24 hours after transcription was induced (Fig 8A-C). However, we did not observe enhanced transcript levels after expression of N protein from MERS-CoV, OC43, 229E, or NL63 (Fig 8A-C), consistent with earlier observations that their expression does not induce PB loss.

303 Taken together, we present the novel finding that three human CoVs induce PB loss and that for
304 SARS-CoV-2, the nucleocapsid protein is responsible for this loss. Moreover, we tested four
305 other CoV N proteins and found that of these, only SARS-CoV-2 N was sufficient to induce PB
306 disassembly and concomitantly enhance levels of selected AU-rich element-containing cytokine
307 mRNAs.
308

Discussion

In this manuscript, we present the first evidence to show that human CoVs, including SARS-CoV-2, induce PB loss after infection. PBs are fundamental sites of post-transcriptional control of gene expression and are particularly relevant to the regulation of cytokine production. Our major findings are as follows. i) Three human coronaviruses, SARS-CoV-2, OC43, and 229E induced PB loss. ii) The SARS-CoV-2 nucleocapsid (N) protein was sufficient to cause PB loss and N protein expression elevated levels of PB-regulated cytokine transcripts encoding IL-6 and TNF. Taken together, these data point to PB loss as a central feature of CoV infection. Moreover, because viral induced PB disassembly elevates PB-regulated cytokine transcripts, this phenotype may contribute to the uncontrolled expression of proinflammatory molecules observed in severe SARS-CoV-2 infection.

We screened 27 SARS-CoV-2 gene products by transfection in HeLa cells [93] and initially identified eight candidate genes that reduced PB numbers (Fig 5). Validation of a subset of these in HUVECs revealed that the most robust and consistent mediator of PB loss was the SARS-CoV-2 viral N protein (Fig 6). The N protein is the most abundant produced protein during CoV replication [96]. The SARS-CoV-2 N protein is 419 amino acids long and has two globular and three intrinsically disordered protein domains, including a central disordered serine-arginine (SR-rich) linker region [96-98]. The N protein is a multifunctional RNA-binding protein (RBP) essential for viral replication; it coats the viral genome and promotes viral particle assembly [46,98-101]. Several recent reports have shown that N protein undergoes liquid-liquid phase separation with RNA, an event which may be regulated by phosphorylation of multiple serine residues in the SR-region and is an important feature of viral assembly[101-106]. The N protein

is also an important modulator of antiviral responses [85,107,108]. A recent study showed that low doses of N protein supressed the production of IFN and some PB-regulated inflammatory cytokines, while high doses of N protein promoted their production [85]. These observations are consistent with our phenotype of PB disassembly, which correlates with later infection times, high expression of N protein and immunofluorescent staining throughout the cytoplasm (Fig 1, Fig 6).

We subsequently screened four other coronavirus N proteins from OC43, MERS, 229E and NL63, and discovered that the phenotype of N-mediated PB disassembly was not conserved among N proteins but was unique to SARS-CoV-2-N (Fig 7). Despite conservation of motifs, the N proteins from different human CoVs possess low sequence conservation at the amino acid level (~50%) and have been reported to exhibit different properties [109]. One key difference that we observed by immunoblotting was the presence of a lower molecular weight ~37 kDa band recognized by our anti-N antibody for SARS-CoV-2. We did not observe the 37kDa N product after OC43 infection, transduction with OC43 N protein or transduction with C-terminally Flag-tagged N proteins from 229E, NL63, or MERS-CoV (Fig 2, Fig 7C). Steady state levels of the ~37 kDa product increased over the course of SARS-CoV-2 infection, consistent with the timing of PB disassembly. Other groups have noted that the SARS-CoV-2 variant of concern (VOC), Alpha (B.1.1.7), produces an additional subgenomic mRNA from which a truncated version of N, termed N*, can be produced [68,110,111]. Translation of the N* ORF is predicted to start at an internal in-frame methionine residue (Met210) within the N protein [110,111] . Alignment of the SARS-CoV-2 N protein sequence against other N proteins revealed that of the human CoVs, only SARS-CoV-1 and SARS-CoV-2 N retained a methionine

355 at position 210 (229E: NC_002645.1, HKU1: NC_006577.2, MERS: NC_019843.3, NL63:
356 NC_005831.2, OC43: NC_006213.1, SARS-1: NC_004718.3, SARS-2: NC_045512.2). Viruses
357 often capitalize on downstream methionine residues to translate truncated protein products with
358 subcellular localization or functions that differ from their full-length counterparts as a clever way
359 to increase coding capacity [112,113]. Our ongoing investigation of the precise nature of the
360 SARS-CoV-2 N protein truncation product we observe during infection and overexpression may
361 reveal that it has a specific role in PB disassembly.
362
363 The PB protein MOV10, and other components of RNA processing machinery, were revealed as
364 potential interactors with the N protein [114]; however, we do not observe colocalization of N
365 protein with PBs after immunofluorescent staining of SARS-CoV-2 infected cells or N-
366 expressing cells. Based on our data, we consider two possible mechanisms of N protein mediated
367 PB disassembly. First, N protein may mediate PB disassembly by phase separation with a PB
368 protein(s). This is similar to what has already been shown for N-mediated disruption of
369 cytoplasmic stress granules, important cytoplasmic biomolecular condensates that correlate with
370 cellular translational shutdown [35]. N protein localizes to stress granules and binds the essential
371 protein, G3BP1, preventing its interaction with other stress granule proteins and blocking stress
372 granule formation [115-117]. Although the precise domain required for this effect has been
373 debated, more than one report suggests that the N-terminal intrinsically disordered region is
374 required for stress granule disruption [116,118]. Second, a possible reason for PB loss may be
375 the indiscriminate binding of RNA by N protein. N protein could be acting as sponge for RNA,
376 pulling it out of cytoplasm, thereby reducing the RNA-protein interactions required for phase
377 separation of PBs [24,115]. We are currently engaged in site-directed and truncation mutagenesis

studies to determine the precise region(s) of SARS-CoV-2- N that is essential for PB disassembly.

Prior to this report, little was known about CoVs and PBs, and the information that was published was contradictory. Infection with murine hepatitis virus (MHV) was reported to increase PBs, whereas transmissible gastroenteritis coronavirus (TGEV) decreased PBs [86,87]. Since the initiation of our study, one additional publication used ectopic expression of one of the SARS-CoV-2 CoV proteases, nsp5, to test if it was capable of PB disassembly. Consistent with the results of our screen (Fig 5), nsp5 did not mediate PB loss [32]. In this manuscript, we now confirm that SARS-CoV-2, OC43, and 229E induce PB disassembly (Fig 1, Fig 2) [34]. We also observed that different human CoVs cause PB loss using different viral gene products; SARS-CoV-2 utilizes N protein but OC43 and 229E do not, a diversity which further underscores that PB disassembly by viruses is intentional and not incidental. Because PBs are composed of numerous cellular molecules with established (e.g. APOBEC, MOV10) or potential (decapping enzymes and exonucleases that could degrade viral RNA) antiviral activities, it is possible that viruses may target PBs for disassembly to negate their antiviral activity [28,29,31,39-45,119]. A recent screen for cellular proteins that bind SARS-CoV-2 viral RNA captured two PB proteins (Lsm14a and MOV10), which suggests CoV RNA may be shuttled to PBs [120]. That said, our evidence does not yet discern if the proposed antiviral role of PB-localized enzymes is promoted by phase separation of molecules into PBs or not; if so, we would predict that the antiviral function of these molecules is lost when PB granules decondense. Emerging evidence suggests that activity of the decapping enzymatic complex is increased by phase separation and decreased in solution [9,24,121]. Thus, we speculate that PBs are direct-acting antiviral granules that can

401 restrict virus infection when present as visible condensates; for this reason, they are targeted for
402 disassembly by most viruses.
403
404 One possibility is that PBs are antiviral because their proteins help the cell respond to signals that
405 activate innate immune pathways [28,30,122,123]. In support of this, TRAF6 was shown to
406 control Dcp1a localization to PBs using ubiquitylation, suggesting that antiviral signaling is
407 more complex than previously appreciated and integrates transcriptional responses with cytokine
408 mRNA suppression in PBs [122,124]. Moreover, the PB protein Lsm14A has been shown to
409 bind to viral RNA/DNA after infection-induced PB disassembly to promote IRF3 activation and
410 IFN-β production [123]. Although it remains unclear if the higher order condensation of many
411 proteins into the PB regulates their proposed antiviral activity, what is clear is that the outcome
412 of PB disassembly is a reversal of the constitutive decay or translational suppression of cytokine
413 mRNAs that would normally occur there [7,12-15,125]. We speculate that when viruses
414 coordinate an attack to cause PB loss, this event is viewed as a danger signal by the cell: it
415 relieves cytokine mRNA suppression and increases the production of proinflammatory cytokines
416 to act as a call for reinforcements. In this way, PB disassembly is connected to the innate
417 immune response and is one of many signals that notify the immune system that a cell is
418 infected. In situations where interferon responses are delayed or defective, as is emerging for
419 SARS-CoV-2 and severe COVID-19 [65-67], PB disassembly may occur to alert the immune
420 system of an infection, and may be an important contributing factor to pathogenic cytokine
421 responses. Ongoing work in our laboratory continues to explore this model of PB regulation of
422 virus infection.
423

In summary, our work adds to a growing body of literature highlighting that many viruses target PBs for disassembly using diverse mechanisms, supporting the idea that PBs restrict viral infection. We showed that the N protein of SARS-CoV-2 is sufficient for PB disassembly and this phenotype correlated with elevated levels of PB-regulated cytokine transcripts encoding IL-6 and TNF. This is significant, as we know that SARS-CoV2 infection is characterized by elevated expression of both these cytokines [53]. Not only does this work describe a previously uncharacterized cellular target of CoV infection, but we have identified a novel mechanism which may contribute to the dysregulated cytokine response exhibited by severe SARS-CoV-2 infection.

Materials and Methods

Cell Culture and Drug Treatments

All cells were maintained in humidified 37 °C incubators with 5% CO_2 and 20% O_2. Vero E6 (ATCC), HEK293T cells (ATCC), HeLa Tet-Off cells (Clontech) and HeLa Flp-In TREx GFP-Dcp1a cells (a generous gift from Anne-Claude Gingras) were cultured in DMEM (Thermo Fisher) supplemented with 100 U/mL penicillin, 100 µg/mL streptomycin, 2 mM L-glutamine (Thermo Fisher) and 10% FBS (Thermo Fisher). Calu3 (ATCC) and MRC-5 cells (ATCC) were cultured in EMEM (ATCC) supplemented with 100 U/mL penicillin, 100 µg/mL streptomycin, 2 mM L-glutamine and 10% FBS. HUVECs (Lonza) were cultured in endothelial cell growth medium (EGM-2) (Lonza). HUVECs were seeded onto tissue culture plates or glass coverslips coated with 0.1 % (w/v) porcine gelatin (Sigma) in 1x PBS. For sodium arsenite treatment, HUVECs were treated with 0.25 mM sodium arsenite (Sigma) or a vehicle control for 30 min.

Plasmids and Cloning

pLenti-IRES-Puro SARS-CoV-2 plasmids were a generous gift from the Krogan Lab [93]. pLJM1-OC43-N was cloned from pGBW-m4134906, a gift from Ginkgo Bioworks & Benjie Chen (Addgene plasmid #151960; http://n2t.net/addgene:151960; RRID:Addgene_151960) using BamHI and EcoRI restriction sites (NEB). pLJM1-NL63-N-FLAG was cloned from pGBW-m4134910, a gift from Ginkgo Bioworks & Benjie Chen (Addgene plasmid #151939; http://n2t.net/addgene:151939; RRID:Addgene_151939) using BamHI and EcoRI. pLJM1-229E-N-FLAG was cloned from pGBW-m4134902, a gift from Ginkgo Bioworks & Benjie Chen (Addgene plasmid #151912; http://n2t.net/addgene:151912; RRID:Addgene_151912) using BamHI and EcoRI. pLJM1-MERS-CoV-N-FLAG was cloned from SinoBiological (cat #VG40068-CF) using BamHI and EcoRI (Table 1).

Transient Transfections

Transient transfections were performed using Fugene (Promega) according to manufacturer's guidelines. Briefly, HeLa Flp-In TREx GFP-Dcp1a cells were seeded in 12-well plates at 150,000 cells/well in antibiotic-free DMEM. Cells were transfected with 1 µg of DNA and 3 µL of Fugene for 48 hours before processing.

Production and use of Recombinant Lentiviruses

All recombinant lentiviruses were generated using a second-generation system. HEK293T cells were transfected with psPAX2, MD2-G, and the lentiviral transfer plasmid containing a gene of interest using polyethylimine (PEI, Polysciences). 6 hours after transfection, serum-free media was replaced with DMEM containing serum but no antibiotics. Viral supernatants were harvested 48 hours post-transfection and frozen at -80°C until use. For transduction, lentiviruses were thawed at 37°C and added to target cells in complete media containing 5 µg/mL polybrene (Sigma). After 24 hours, the media was replaced with selection media containing 1 µg/mL puromycin or 5 µg/mL blasticidin (ThermoFisher) and cells were selected for 48 h before proceeding with experiments.

Immunofluorescence

Cells were seeded onto 18mm round, #1.5 coverslips (Electron Microscopy Sciences) for immunofluorescence experiments. Following treatment, cells were fixed for 10 or 30 (if infected with SARS-CoV-2) min in 4% (v/v) paraformaldehyde (Electron Microscopy Sciences). Samples were permeabilized with 0.1% (v/v) Triton X-100 (Sigma-Aldrich) for 10 min at room temperature and blocked in 1% human AB serum (Sigma-Aldrich) in 1X PBS 1 h at room temperature. Primary and secondary antibodies (Table 2) were diluted in 1% human AB serum and used at the concentrations in Table 2. Nuclei were stained with 1 µg/ml Hoechst

(Invitrogen). Samples were mounted with Prolong Gold AntiFade mounting media (ThermoFisher).

Immunoblotting

Cells were lysed in 2X Laemmli buffer and stored at -20°C until use. The DC Protein Assay (Bio-Rad) was used to quantify protein concentration as per the manufacturer's instructions. 10-15 µg of protein lysate was resolved by SDS-PAGE on TGX Stain-Free acrylamide gels (BioRad). Total protein images were acquired from the PVDF membranes after transfer on the ChemiDoc Touch Imaging system (BioRad). Membranes were blocked in 5% BSA in TBS-T (Tris-buffered saline 0.1% Tween-20). Primary and secondary antibodies were diluted in 2.5% BSA, dilutions can be found in Table 2. Membranes were visualized using Clarity Western ECL substrate and the ChemiDoc Touch Imaging system (BioRad).

Quantitative PCR

RNA was collected using the RNeasy Plus Mini Kit (Qiagen) according to the manufacturer's instructions and stored at -80°C until further use. RNA concentration was determined using NanoDrop One^{C} (ThermoFisher) and 500 ng of RNA was reverse transcribed using qScript XLT cDNA SuperMix (QuantaBio) using a combination of random hexamer and oligo dT primers, according to the manufacturer's instructions. Depending on starting concentration, cDNA was diluted between 1:10 and 1:20 for qPCR experiments and SsoFast EvaGreen Mastermix (Biorad) was used to amplify cDNA. The ΔΔquantitation cycle (Cq) method was used to determine the fold change in expression of target transcripts. qPCR primer sequences can be found in Table 3.

Virus Propagation

Experiments with SARS-CoV-2 were conducted in a containment level-3 (CL3) facility, and all standard operating procedures were approved by the CL3 Oversight Committee and Biosafety

Office at the University of Calgary. Stocks of SARS-CoV-2 Toronto-01 isolate [126] were propagated in Vero E6 cells. To produce viral stocks, Vero E6 cells were infected at an MOI of 0.01 for 1 hour in serum-free DMEM at 37˚C. Following adsorption, DMEM supplemented with 2% heat inactivated FBS and 100 U/mL penicillin/streptomycin/glutamine was added to the infected wells. 24-48 days post-infection (dpi), the supernatant was harvested and centrifuged at 500 x *g* for 5 min to remove cellular debris. Virus stocks were aliquoted and stored at -80˚C for single use. SARS-CoV-2 titres were enumerated using plaque assays on Vero E6 cells as previously described [127]using equal parts 2.4% w/v semi-solid colloidal cellulose overlay (Sigma; prepared in ddH_2O) and 2X DMEM (Wisent) with 1% heat inactivated FBS and 1% PSQ.

Experiments with hCoV-OC43 (ATCC VR-1558) and hCoV-229E (ATCC VR-740) were conducted in under containment level-2 conditions. hCoV-OC43 and hCoV-229E were propagated in Vero E6 and MRC-5 cells, respectively. Cells were infected at an MOI of 0.01 for 1 hour in serum-free media at 33˚C. Following adsorption, the viral inoculum was removed and replaced with fresh media supplemented with 2% heat inactivated FBS and 100 U/mL penicillin/streptomycin/glutamine. After 5-6 dpi, the supernatant was harvested and cellular debris was cleared by centrifugation. Virus stocks were aliquoted and stored at -80˚C. hCoV-OC43 and hCoV-229E titres were enumerated using Reed and Muench tissue-culture infectious dose 50% ($TCID_{50}$) in Vero E6 or MRC-5 cells, respectively.

Virus Infection

For experimental infections, cells were seeded into wells to achieve ~80% confluency at the time of infection. The growth media was removed and replaced with 100 µL of viral inoculum diluted in serum-free DMEM to reach the desired MOI and incubated at 37˚C for 1 hour, rocking the

plate every 10 min. Following incubation, the virus inoculum was removed and replaced with 1 mL of complete grown media.

Processing Body Quantification

Processing bodies were quantified using an unbiased image analysis pipeline generated in the freeware CellProfiler (cellprofiler.org) [128] described in more detail in [90]. First, nuclear staining was used to identify individual cells applying a binary threshold and executing primary object detection between 50 and 250 pixels. For each identified object (the nucleus), the peripheral boundary of each cell was defined using the "Propagation" function. Using a subtractive function to remove the nuclei from the total cell area, the cytoplasm of each cell was defined. The cytoplasm area mask was then applied to the matched image stained for PB proteins (DDX6 or Hedls) to count only DDX6 or Hedls-positive cytoplasmic puncta. Only the cytoplasms of "positive" staining cells (e.g. SARS-CoV-2 N protein channel) were quantified unless otherwise indicated in corresponding figure legends. Background staining was reduced using the "Enhance Speckles" function. Only DDX6 or Hedls-positive puncta with a defined size and intensity range were quantified using "global thresholding with robust background adjustments" function. All thresholds were consistent between experiments that used identical staining parameters. For Figure 5, puncta counts were exported and RStudio was used for data analysis.

Statistics

All statistical analyses were performed using GraphPad Prism 9.0. Significance was determined using a paired Student's t-test unless otherwise indicated in corresponding figure legends.

551

552 **Table 1: Plasmids**

Plasmid	Use	Source	Mammalian Selection
pLJM1-Puro	Empty Vector Control	[90] [129]	Puromycin
pLJM1-BSD	Empty Vector Control	[129]	Blasticidin
pLJM1-ACE2	Overexpression		Blasticidin
pMD2.G	Lentivirus Generation	Addgene #12259	N/A
psPAX2	Lentivirus Generation	Addgene #12260	N/A
pLJM1-OC43-N	Overexpression	Addgene #151960	Puromycin
pLJM1-229E-N-FLAG	Overexpression	Addgene #151912	Puromycin
pLJM1-NL63-N-FLAG	Overexpression	Addgene #151939	Puromycin
pLJM1-MERS-CoV-N-FLAG	Overexpression	SinoBiological #VG40068-CF	Puromycin
pLenti-SARS-CoV-2-IRES-strep	Overexpression library	N Krogan (UCSF) [114]	Puromycin

553

554

555

556

557

558

559

560

561

562

563

564

Table 2: Antibodies

Antibody	Species	Vendor/Catalog #	Application	Dilution
Strep-Tag II	Mouse	Sigma (71590-M)	Immunofluorescence Immunoblot	1:1000 1:1000
DDX6	Rabbit	Bethyl (A300-461)	Immunofluorescence Immunoblot	1:1000 1:1000
Hedls	Mouse	Santa Cruz (sc-8418)	Immunofluorescence Immunoblot	1:1000 1:1000
Dcp1a	Rabbit	Novus (H00055802-M06)	Immunoblot	1:1000
Xrn1	Mouse	Abcam (ab231197)	Immunoblot	1:1000
Coronavirus OC43 Nucleocapsid	Mouse	Millipore (MAB-9012)	Immunofluorescence Immunoblot	1:500 1:1000
SARS-CoV2 Nucleocapsid	Rabbit	Novus (NBP3-05730)	Immunofluorescence	1:1000
SARS-CoV2 Nucleocapsid	Mouse	Novus (NBP3-05706)	Immunofluorescence Immunoblot	1:1000 1:1000
dsRNA clone J2	Mouse	Millipore (MABE-1134)	Immunofluorescence	1:100
FLAG	Mouse	CST (8146)	Immunofluorescence Immunoblot	1:1000 1:1000
Actin HRP-conjugated	Rabbit	CST (5215)	Immunoblot	1:10,000

581 **Table 3: qPCR primers**

Target	Direction	Sequence 5'→3'
HPRT	Forward	CTTTCCTTGGTCAGGCAGTATAA
HPRT	Reverse	AGTCTGGCTTATATCCAACACTTC
18S	Forward	TTCGAACGTCTGCCCTATCAA
18S	Reverse	GATGTGGTAGCCGTTTCTCAGG
IL6	Forward	GAAGCTCTATCTCGCCTCCA
IL6	Reverse	TTTTCTGCCAGTGCCTCTTT
CXCL8	Forward	AAATCTGGCAACCCTAGTCTG
CXCL8	Reverse	GTGAGGTAAGATGGTGGCTAAT
IL-1β	Forward	CTCTCACCTCTCCTACTCACTT
IL-1β	Reverse	TCAGAATGTGGGAGCGAATG
TNF	Forward	TCGAACCCCGAGTGACAA
TNF	Reverse	AGCTGCCCCTCAGCTTG
GM-CSF	Forward	AAATGTTTGACCTCCAGGAGCC
GM-CSF	Reverse	ATCTGGGTTGCACAGGAAGTT
COX-2	Forward	CCCTTGGGTGTCAAAGGTAA
COX-2	Reverse	GCCCTCGCTTATGATCTGTC

582

583

584 **Figure Legends**

585

586 **Figure 1. Processing bodies are absent in SARS-CoV-2 infected cells. A.** HUVECs were
587 transduced with recombinant lentiviruses expressing human ACE2, selected, and infected with
588 SARS-CoV-2 TO-1 isolate at an MOI of 3. At 6 or 24 hours post infection (hpi), virus-
589 containing supernatant was harvested and titered by $TCID_{50}$ assay. *n*=2. **B-E.** HUVEC-ACE2
590 cells were infected with SARS-CoV-2 (MOI = 3) or mock-infected. At 16 hpi or 24 hpi, cells
591 were fixed and immunostained for SARS-CoV-2 N protein (green) and either DDX6 (B, white)
592 or Hedls (D, white). Nuclei were stained with Hoechst (blue). DDX6 puncta (C) and Hedls
593 puncta (E) in mock or SARS-CoV-2-infected cells were quantified using CellProfiler and is
594 expressed as fold-change relative to mock. *n*=3; mean ± SD (*, $P < 0.05$; ***, $P < 0.001$). **G.**
595 Calu3 cells were infected with SARS-CoV-2 (MOI =2) or mock-infected. 48 hours later, cells
596 were fixed and immunostained for SARS-CoV-2 N (green), DDX6 (PBs; white). Nuclei were
597 stained with Hoechst (blue). Representative images from one of two independent experiments
598 are shown. *n*=2. Scale bar = 20 µm.

599 **Figure 2. Processing bodies are absent in OC43 and 229E infected cells. A-B.** Each well of
600 12-well plate of HUVECs were infected with OC43 ($TCID_{50} = 2 \times 10^4$) or 229E ($TCID_{50} = 2.4 \times$
601 10^3). Supernatants were harvested at 6, 12, and 24 hpi and titrated by $TCID_{50}$ on Vero E6 or
602 MRC5 cells for OC43 or 229E, respectively. *n*=2; mean ± SD. **C.** HUVECs were infected with
603 OC43 or mock-infected, fixed at 12 hpi or 24 hpi and immunostained for DDX6 (PBs; white)
604 and OC43 N protein (green). Nuclei were stained with Hoechst (blue) **D.** DDX6 puncta in mock
605 or OC43-infected cells were quantified as in Figure 1. *n*=3, mean ± SD (**, $P < 0.01$). **E.** Each
606 well of 12-well plate of HUVECs were infected with 229E ($TCID_{50} = 2.4 \times 10^3$) or mock-

607 infected, fixed at 6 hpi or 12 hpi and immunostained for DDX6 (white) or dsRNA (green).
608 Nuclei were stained with Hoechst (blue). **F.** DDX6 puncta in mock or 229E-infected cells as in
609 Figure 1. *n*=3; mean ± SD (*, P < 0.05; ns, nonsignificant). Scale bar = 20 μm.

610 **Figure 3. Coronavirus infection does not alter steady state levels of processing body**
611 **proteins. A.** HUVECs were transduced with human ACE2, selected, and infected with SARS-
612 CoV-2 at an MOI of 3. Cells were lysed at 6 and 12 hpi and immunoblotting was performed
613 using XRN1, Hedls, DCP1A, DDX6, SARS-Cov-2 N, and β-actin specific antibodies. One
614 representative experiment of three is shown. **B-C.** Each well of 12-well plate of HUVECs were
615 infected with OC43 (B, $TCID_{50} = 2 \times 10^4$) or 229E (C, $TCID_{50} = 2.4 \times 10^3$). Cells were lysed at
616 12 and 24hpi (B, OC43) or 6 and 12 hpi (C, 229E). Immunoblotting was performed using XRN1,
617 Hedls, DCP1A, DDX6, OC43 N protein (B only), and β-actin specific antibodies. One
618 representative experiment of three is shown.
619
620 **Figure 4. Steady state levels of selected ARE-mRNAs are elevated during coronavirus**
621 **infection. A.** HUVECs were transduced with recombinant lentiviruses expressing human ACE2,
622 selected, and infected with SARS-CoV-2 (MOI=3). RNA was harvested 24 hpi and RT-qPCR
623 was performed using IL-6, CXCL8, COX-2, GM-CSF, IL-1β and HPRT specific primers. Values
624 are represented as fold change relative to mock-infection. *n*=3; mean ± SD (*, P < 0.05; **, P <
625 0.01; ns, nonsignificant). **B-C.** HUVECs were infected with OC43 (B, $TCID_{50}/mL = 3.5 \times 10^4$)
626 or 229E (C, $TCID_{50}/mL = 1 \times 10^{3.24}$). RNA was harvested 24 and 12 hpi for OC43 (B) and 229E
627 (C), respectively, and RT-qPCR was performed as in (A). Values are represented as fold change
628 relative to mock-infection. *n*≥3; mean ± SD (*, P < 0.05; **, P < 0.01; ns, nonsignificant).
629

Figure 5. Identification of SARS-CoV-2 ORFs that mediate processing body loss. A-C HeLa cells expressing GFP-Dcp1a were transfected with an empty vector or 2xStrep-tagged SARS-CoV-2 ORFs for 48 hours then fixed and immunostained for Strep-tag (red) or DDX6 (white). Nuclei were stained with Hoechst (blue). **A.** Select ORFs are shown; Scale bar = 20 μm. **B-C.** DDX6 puncta were quantified using CellProfiler. In B, SARS-CoV-2 ORF-expressing cells were thresholded by Strep-tag staining intensity. The intensity threshold used was defined as two standard deviations above mean intensity in vector controls. Only DDX6 puncta in cells above this threshold were counted. In C, transfected cells did not stain above this threshold; therefore, DDX6 puncta in all cells were counted. Values are expressed as a fold-change difference normalized to the vector control (hashed line). A one-way ANOVA with a Dunnett's post-hoc analysis was performed, n=3; bars represent SEM; **=P<0.01. **D.** HeLa cells were transfected as above for 48 hours and lysates were harvested in 2x Laemmli buffer. Samples were resolved by SDS-PAGE on 4-15% gradient gels (BioRad) and immunoblotted with a Strep-Tag II antibody (Sigma).

Figure 6. Ectopic expression of SARS-CoV-2 N elicits processing body disassembly. A. HUVECs were transduced with recombinant lentiviruses ectopically expressing 2xStrep-tagged SARS-CoV-2 N or controls and selected with puromycin for 48 hours. Samples were fixed and immunostained for Strep-tag (green) and DDX6 (white). Nuclei were stained with Hoechst (blue). Scale bar = 20 μm. **B.** DDX6 puncta were quantified per field of view using CellProfiler as in Figure 1. Values are expressed as fold-change normalized to the control transduction; *n*=3; mean ± SD (*, P < 0.05). **C-F.** HUVECs were transduced and selected as in A, then treated with 0.25 mM sodium arsenite or a vehicle control for 30 min, fixed and immunostained for either

653 Hedls (C, white) or DDX6 (D, white) and SARS-CoV-2 N (green). Nuclei were stained with
654 Hoechst (blue). Scale bar = 20 μm. Hedls puncta (D) and DDX6 puncta (F) were quantified per
655 field of view as in (B). *n*=2; mean ± SD.
656
657 **Figure 7. Processing body disassembly is not a common feature of all human coronavirus N**
658 **proteins. A.** HUVECs were transduced recombinant lentiviruses ectopically expressing N
659 protein from the betacoronaviruses MERS-CoV, OC43 or control lentiviruses. SARS-CoV-2 N
660 protein expressing lentiviruses were used as a positive control. Cells were selected, fixed and
661 immunostained for DDX6 (white) and either authentic N protein or a FLAG tag (green). Nuclei
662 were stained with Hoechst (blue). Scale bar = 20 μm. **B.** DDX6 puncta in EV or N-transduced
663 cells were quantified per field of view by CellProfiler and represented as fold-change relative to
664 EV-transduced cells. A one-way ANOVA with a Dunnett's post-hoc analysis was performed;
665 *n*=3; mean ± SD (**, $P < 0.01$; ns, nonsignificant). **C.** HUVECs were transduced with
666 recombinant lentiviruses ectopically expressing N protein from the alphacoronaviruses 229E,
667 NL63 or control lentiviruses. SARS-CoV-2 N protein expressing lentiviruses were used as a
668 positive control. Cells were fixed and immunostained as in (A). Scale bar = 20 μm. **D.** DDX6
669 puncta in EV or N-transduced cells were quantified per field of view by CellProfiler and
670 represented as fold-change relative to EV-transduced cells. A one-way ANOVA with a
671 Dunnett's post-hoc analysis was performed; *n*=3; mean ± SD (*, $P < 0.05$; ns, nonsignificant). **E-**
672 **F.** HUVECs were transduced as in A and C, respectively, harvested in 2x Laemmli buffer and
673 immunoblotting was performed using XRN1, Hedls, DCP1A, DDX6, N protein or FLAG, and β-
674 actin specific antibodies. One representative experiment of three is shown.
675

Figure 8. Ectopic expression of SARS-CoV-2 N elevates selected ARE-mRNAs. A-C. HUVECs were transduced with recombinant lentiviruses ectopically expressing alpha- and betacoronavirus N proteins or empty vector (EV) control, selected, and treated with 0.01 ng/L soluble TNF to increase transcription of ARE-containing cellular mRNAs. Total RNA was harvested at 0, 8, 12, and 24 hours post TNF treatment and RT-qPCR was performed using IL-6 (A), CXCL8 (B), TNF (C) and HPRT specific primers. Values are represented as fold-change relative to EV-transduced cells for each time point. A one-way ANOVA with a Dunnett's post-hoc analysis was performed; n=3; mean ± SD (*, $P < 0.05$).

Supplemental Figure Legends

Figure S1. ACE2 expression does not alter processing body numbers. A-B. HUVECs were transduced with recombinant lentiviruses expressing human ACE2 or an empty vector (EV) control, selected, fixed and immunostained for the PB-resident proteins Hedls (A) and DDX6 (B). Puncta were quantified using CellProfiler and normalized to control (EV) counts. n=2; mean ± SD.

Figure S2. Ectopic expression of four SARS-CoV-2 ORFs mediates processing body loss. A. HUVECs were transduced recombinant lentiviruses expressing 2xStrep-tagged SARS-CoV-2 nsp1, nsp14, ORF3b and ORF7b constructs or control lentiviruses and selected with puromycin for 48 h. Samples were fixed and immunostained for Strep-tag (red) or DDX6 (white). Nuclei were stained with Hoechst (blue). Scale bar = 20 μm. **B.** DDX6 puncta were quantified per field

699 of view using CellProfiler and expressed as a fold-change normalized to the empty vector
700 control; *n*=2; mean ± SD. **C**. HUVECs were transduced in (A). Lysates were harvested in 2x
701 Laemmli buffer. Samples were resolved by SDS-PAGE on 4-15% gradient gels (BioRad) and
702 immunoblotted with a Strep-Tag II antibody (Sigma).
703
704

Acknowledgements

We sincerely thank the members of the Corcoran lab for helpful discussions about this work. We would like to thank Dr. Nevan Krogan (UCSF) for sharing the SARS-CoV-2 gene library. We would like to thank Dr. Anne Vaahtokari of the Charbonneau Microscopy Facility for microscopy support and Dr. Devender Kumar for CL3 facility support. MK was supported by a CSM graduate training award, a CIHR CGS-M scholarship, and a CIHR doctoral award. Operating funds to support this work derive from the Canadian Institutes of Health Research. The Vaccine and Infectious Disease Organization (VIDO) receives operational funding for its CL3 facility (InterVac) from the Canada Foundation for Innovation through the Major Science Initiatives. VIDO also receives operational funding from the Government of Saskatchewan through Innovation Saskatchewan and the Ministry of Agriculture.

Author Contributions

Mariel Kleer: Conceptualization, Experimentation, Analysis, Paper Writing

Rory P. Mulloy: Conceptualization, Experimentation, Analysis, Paper Writing

Carolyn-Ann Robinson: Conceptualization, Experimentation, Analysis, Paper Writing

Elizabeth L. Castle: Analysis

Maxwell Bui-Marinos: Experimentation, Paper Writing

Jennifer A. Corcoran: Conceptualization, Experimentation, Supervision, Funding Acquisition, Project Administration, Paper Writing

Conflict of Interest

The authors have no competing interests to declare.

728 **References**

729 1. Eulalio A, Behm-Ansmant I, Schweizer D, Izaurralde E. P-body formation is a
730 consequence, not the cause, of RNA-mediated gene silencing. Mol Cell Biol. 2007;27:
731 3970–3981. doi:10.1128/MCB.00128-07

732 2. Eulalio A, Rehwinkel J, Stricker M, Huntzinger E, Yang S-F, Doerks T, et al. Target-
733 specific requirements for enhancers of decapping in miRNA-mediated gene silencing.
734 Genes Dev. Cold Spring Harbor Lab; 2007;21: 2558–2570. doi:10.1101/gad.443107

735 3. Hubstenberger A, Courel M, Bénard M, Souquere S, Ernoult-Lange M, Chouaib R, et al.
736 P-Body Purification Reveals the Condensation of Repressed mRNA Regulons. Mol Cell.
737 Elsevier Inc; 2017;68: 144–157.e5. doi:10.1016/j.molcel.2017.09.003

738 4. Youn J-Y, Dunham WH, Hong SJ, Knight JDR, Bashkurov M, Chen GI, et al. High-
739 Density Proximity Mapping Reveals the Subcellular Organization of mRNA-Associated
740 Granules and Bodies. Mol Cell. Elsevier Inc; 2018;69: 517–532.e11.
741 doi:10.1016/j.molcel.2017.12.020

742 5. Bakheet T, Hitti E, Khabar KSA. ARED-Plus: an updated and expanded database of
743 AU-rich element-containing mRNAs and pre-mRNAs. Nucleic Acids Research.
744 2018;46: D218–D220. doi:10.1093/nar/gkx975

745 6. Hitti E, Bakheet T, Al-Souhibani N, Moghrabi W, Al-Yahya S, Al-Ghamdi M, et al.
746 Systematic Analysis of AU-Rich Element Expression in Cancer Reveals Common
747 Functional Clusters Regulated by Key RNA-Binding Proteins. Cancer Res. 2016;76:
748 4068–4080. doi:10.1158/0008-5472.CAN-15-3110

749 7. Blanco FF, Sanduja S, Deane NG, Blackshear PJ, Dixon DA. Transforming growth
750 factor β regulates P-body formation through induction of the mRNA decay factor
751 tristetraprolin. Mol Cell Biol. 2014;34: 180–195. doi:10.1128/MCB.01020-13

752 8. Brengues M, Teixeira D, Parker R. Movement of eukaryotic mRNAs between
753 polysomes and cytoplasmic processing bodies. Science. American Association for the
754 Advancement of Science; 2005;310: 486–489. doi:10.1126/science.1115791

755 9. Riggs CL, Kedersha N, Ivanov P, Anderson P. Mammalian stress granules and P bodies
756 at a glance. J Cell Sci. 2020;133: jcs242487. doi:10.1242/jcs.242487

757 10. Khong A, Parker R. mRNP architecture in translating and stress conditions reveals an
758 ordered pathway of mRNP compaction. J Cell Biol. 2018;217: 4124–4140.
759 doi:10.1083/jcb.201806183

760 11. Matheny T, Rao BS, Parker R. Transcriptome-Wide Comparison of Stress Granules and
761 P-Bodies Reveals that Translation Plays a Major Role in RNA Partitioning. Mol Cell
762 Biol. 2019;39: 612. doi:10.1128/MCB.00313-19

12. Corcoran JA, Khaperskyy DA, Johnston BP, King CA, Cyr DP, Olsthoorn AV, et al. Kaposi's sarcoma-associated herpesvirus G-protein-coupled receptor prevents AU-rich-element-mediated mRNA decay. J Virol. 2012;86: 8859–8871. doi:10.1128/JVI.00597-12

13. Corcoran JA, Johnston BP, McCormick C. Viral Activation of MK2-hsp27-p115RhoGEF-RhoA Signaling Axis Causes Cytoskeletal Rearrangements, P-body Disruption and ARE-mRNA Stabilization. Robertson ES, editor. PLoS Pathogens. Public Library of Science; 2015;11: e1004597. doi:10.1371/journal.ppat.1004597

14. Franks TM, Lykke-Andersen J. TTP and BRF proteins nucleate processing body formation to silence mRNAs with AU-rich elements. Genes Dev. 2007;21: 719–735. doi:10.1101/gad.1494707

15. Vindry C, Marnef A, Broomhead H, Twyffels L, Ozgur S, Stoecklin G, et al. Dual RNA Processing Roles of Pat1b via Cytoplasmic Lsm1-7 and Nuclear Lsm2-8 Complexes. CellReports. 2017;20: 1187–1200. doi:10.1016/j.celrep.2017.06.091

16. Vandelli A, Cid Samper F, Torrent Burgas M, Sanchez de Groot N, Tartaglia GG. The Interplay Between Disordered Regions in RNAs and Proteins Modulates Interactions Within Stress Granules and Processing Bodies. J Mol Biol. 2021;: 167159. doi:10.1016/j.jmb.2021.167159

17. Nosella ML, Forman-Kay JD. Phosphorylation-dependent regulation of messenger RNA transcription, processing and translation within biomolecular condensates. Curr Opin Cell Biol. 2021;69: 30–40. doi:10.1016/j.ceb.2020.12.007

18. Jalihal AP, Pitchiaya S, Xiao L, Bawa P, Jiang X, Bedi K, et al. Multivalent Proteins Rapidly and Reversibly Phase-Separate upon Osmotic Cell Volume Change. Mol Cell. 2020;79: 978–990.e5. doi:10.1016/j.molcel.2020.08.004

19. Mitrea DM, Chandra B, Ferrolino MC, Gibbs EB, Tolbert M, White MR, et al. Methods for Physical Characterization of Phase-Separated Bodies and Membrane-less Organelles. J Mol Biol. 2018;430: 4773–4805. doi:10.1016/j.jmb.2018.07.006

20. Banani SF, Rice AM, Peeples WB, Lin Y, Jain S, Parker R, et al. Compositional Control of Phase-Separated Cellular Bodies. Cell. 2016;166: 651–663. doi:10.1016/j.cell.2016.06.010

21. Guillén-Boixet J, Kopach A, Holehouse AS, Wittmann S, Jahnel M, Schlüßler R, et al. RNA-Induced Conformational Switching and Clustering of G3BP Drive Stress Granule Assembly by Condensation. Cell. 2020;181: 346–361.e17. doi:10.1016/j.cell.2020.03.049

22. Van Treeck B, Parker R. Emerging Roles for Intermolecular RNA-RNA Interactions in RNP Assemblies. Cell. 2018;174: 791–802. doi:10.1016/j.cell.2018.07.023

799 23. Cougot N, Cavalier A, Thomas D, Gillet R. The dual organization of P-bodies revealed
800 by immunoelectron microscopy and electron tomography. J Mol Biol. 2012;420: 17–28.
801 doi:10.1016/j.jmb.2012.03.027

802 24. Corbet GA, Parker R. RNP Granule Formation: Lessons from P-Bodies and Stress
803 Granules. Cold Spring Harb Symp Quant Biol. 2019;84: 203–215.
804 doi:10.1101/sqb.2019.84.040329

805 25. Standart N, Weil D. P-Bodies: Cytosolic Droplets for Coordinated mRNA Storage.
806 Trends Genet. 2018;34: 612–626. doi:10.1016/j.tig.2018.05.005

807 26. Docena G, Rovedatti L, Kruidenier L, Fanning A, Leakey NAB, Knowles CH, et al.
808 Down-regulation of p38 mitogen-activated protein kinase activation and
809 proinflammatory cytokine production by mitogen-activated protein kinase inhibitors in
810 inflammatory bowel disease. Clin Exp Immunol. John Wiley & Sons, Ltd; 2010;162:
811 108–115. doi:10.1111/j.1365-2249.2010.04203.x

812 27. Jangra RK, Yi M, Lemon SM. DDX6 (Rck/p54) is required for efficient hepatitis C
813 virus replication but not for internal ribosome entry site-directed translation. J Virol.
814 2010;84: 6810–6824. doi:10.1128/JVI.00397-10

815 28. Ng CS, Kasumba DM, Fujita T, Luo H. Spatio-temporal characterization of the antiviral
816 activity of the XRN1-DCP1/2 aggregation against cytoplasmic RNA viruses to prevent
817 cell death. Cell Death & Differentiation. Nature Publishing Group; 2020;36: 932–20.
818 doi:10.1038/s41418-020-0509-0

819 29. Ostareck DH, Naarmann-de Vries IS, Ostareck-Lederer A. DDX6 and its orthologs as
820 modulators of cellular and viral RNA expression. Wiley Interdiscip Rev RNA. 2014;5:
821 659–678. doi:10.1002/wrna.1237

822 30. Dougherty JD, Tsai W-C, Lloyd RE. Multiple Poliovirus Proteins Repress Cytoplasmic
823 RNA Granules. Viruses. Multidisciplinary Digital Publishing Institute; 2015;7: 6127–
824 6140. doi:10.3390/v7122922

825 31. Dougherty JD, White JP, Lloyd RE. Poliovirus-mediated disruption of cytoplasmic
826 processing bodies. J Virol. 2011;85: 64–75. doi:10.1128/JVI.01657-10

827 32. Fan S, Xu Z, Liu P, Qin Y, Chen M. Enterovirus 71 2A Protease Inhibits P-Body
828 Formation To Promote Viral RNA Synthesis. J Virol. 2021;95: e0092221.
829 doi:10.1128/JVI.00922-21

830 33. Kanakamani S, Suresh PS, Venkatesh T. Regulation of processing bodies: From viruses
831 to cancer epigenetic machinery. Cell Biol Int. John Wiley & Sons, Ltd; 2021;45: 708–
832 719. doi:10.1002/cbin.11527

833 34. Gaete-Argel A, Márquez CL, Barriga GP, Soto-Rifo R, Valiente-Echeverría F.
834 Strategies for Success. Viral Infections and Membraneless Organelles. Front Cell Infect
835 Microbiol. 2019;9: 336. doi:10.3389/fcimb.2019.00336

35. McCormick C, Khaperskyy DA. Translation inhibition and stress granules in the antiviral immune response. Nature Reviews Immunology. Nature Publishing Group; 2017;17: 647–660. doi:10.1038/nri.2017.63

36. Tsai W-C, Lloyd RE. Cytoplasmic RNA Granules and Viral Infection. Annu Rev Virol. Annual Reviews; 2014;1: 147–170. doi:10.1146/annurev-virology-031413-085505

37. Onomoto K, Jogi M, Yoo J-S, Narita R, Morimoto S, Takemura A, et al. Critical role of an antiviral stress granule containing RIG-I and PKR in viral detection and innate immunity. Kanai A, editor. PLoS ONE. Public Library of Science; 2012;7: e43031. doi:10.1371/journal.pone.0043031

38. Abernathy E, Gilbertson S, Alla R, Glaunsinger B. Viral Nucleases Induce an mRNA Degradation-Transcription Feedback Loop in Mammalian Cells. Cell Host and Microbe. 2015;18: 243–253. doi:10.1016/j.chom.2015.06.019

39. Núñez RD, Budt M, Saenger S, Paki K, Arnold U, Sadewasser A, et al. The RNA Helicase DDX6 Associates with RIG-I to Augment Induction of Antiviral Signaling. Int J Mol Sci. Multidisciplinary Digital Publishing Institute; 2018;19: 1877. doi:10.3390/ijms19071877

40. Balinsky CA, Schmeisser H, Wells AI, Ganesan S, Jin T, Singh K, et al. IRAV (FLJ11286), an Interferon-Stimulated Gene with Antiviral Activity against Dengue Virus, Interacts with MOV10. Diamond MS, editor. J Virol. 2017;91: 504. doi:10.1128/JVI.01606-16

41. Wang H, Chang L, Wang X, Su A, Feng C, Fu Y, et al. MOV10 interacts with Enterovirus 71 genomic 5'UTR and modulates viral replication. Biochem Biophys Res Commun. 2016;479: 571–577. doi:10.1016/j.bbrc.2016.09.112

42. Cuevas RA, Ghosh A, Wallerath C, Hornung V, Coyne CB, Sarkar SN. MOV10 Provides Antiviral Activity against RNA Viruses by Enhancing RIG-I-MAVS-Independent IFN Induction. J Immunol. 2016;196: 3877–3886. doi:10.4049/jimmunol.1501359

43. Burdick R, Smith JL, Chaipan C, Friew Y, Chen J, Venkatachari NJ, et al. P body-associated protein Mov10 inhibits HIV-1 replication at multiple stages. J Virol. 2010;84: 10241–10253. doi:10.1128/JVI.00585-10

44. Burgess HM, Mohr I. Cellular 5“-3” mRNA exonuclease Xrn1 controls double-stranded RNA accumulation and anti-viral responses. Cell Host and Microbe. 2015;17: 332–344. doi:10.1016/j.chom.2015.02.003

45. Lumb JH, Li Q, Popov LM, Ding S, Keith MT, Merrill BD, et al. DDX6 Represses Aberrant Activation of Interferon- Stimulated Genes. CellReports. ElsevierCompany; 2017;20: 819–831. doi:10.1016/j.celrep.2017.06.085

46. V'kovski P, Kratzel A, Steiner S, Stalder H, Thiel V. Coronavirus biology and replication: implications for SARS-CoV-2. Nat Rev Microbiol. Nature Publishing Group; 2020;5: 536–16. doi:10.1038/s41579-020-00468-6

47. Cui J, Li F, Shi Z-L. Origin and evolution of pathogenic coronaviruses. Springer US; 2019;: 1–12. doi:10.1038/s41579-018-0118-9

48. Banerjee A, Doxey AC, Tremblay BJ-M, Mansfield MJ, Subudhi S, Hirota JA, et al. Predicting the recombination potential of severe acute respiratory syndrome coronavirus 2 and Middle East respiratory syndrome coronavirus. J Gen Virol. Microbiology Society; 2020;101: 1251–1260. doi:10.1099/jgv.0.001491

49. Banerjee A, Doxey AC, Mossman K, Irving AT. Unraveling the Zoonotic Origin and Transmission of SARS-CoV-2. Trends Ecol Evol. 2021;36: 180–184. doi:10.1016/j.tree.2020.12.002

50. Zhou H, Ji J, Chen X, Bi Y, Li J, Wang Q, et al. Identification of novel bat coronaviruses sheds light on the evolutionary origins of SARS-CoV-2 and related viruses. Cell. 2021;184: 4380–4391.e14. doi:10.1016/j.cell.2021.06.008

51. Li W, Shi Z, Yu M, Ren W, Smith C, Epstein JH, et al. Bats are natural reservoirs of SARS-like coronaviruses. Science. American Association for the Advancement of Science; 2005;310: 676–679. doi:10.1126/science.1118391

52. Fielding CA, Jones GW, McLoughlin RM, McLeod L, Hammond VJ, Uceda J, et al. Interleukin-6 signaling drives fibrosis in unresolved inflammation. Immunity. 2014;40: 40–50. doi:10.1016/j.immuni.2013.10.022

53. Blanco-Melo D, tenover BR. Imbalanced host response to SARS-CoV-2 drives development of COVID-19. Cell. 2020;: 1–46. doi:10.1016/j.cell.2020.04.026

54. Pedersen SF, Ho Y-C. SARS-CoV-2: a storm is raging. Journal of Clinical Investigation. 2020;130: 2202–2205. doi:10.1172/JCI137647

55. Zou L, Ruan F, Huang M, Liang L, Huang H, Hong Z, et al. SARS-CoV-2 Viral Load in Upper Respiratory Specimens of Infected Patients. N Engl J Med. Massachusetts Medical Society; 2020;382: 1177–1179. doi:10.1056/NEJMc2001737

56. Libby P, Lüscher T. COVID-19 is, in the end, an endothelial disease. Eur Heart J. 3rd ed. 2020;41: 3038–3044. doi:10.1093/eurheartj/ehaa623

57. Chen G, Wu D, Guo W, Cao Y, Huang D, Wang H, et al. Clinical and immunological features of severe and moderate coronavirus disease 2019. J Clin Invest. American Society for Clinical Investigation; 2020;130: 2620–2629. doi:10.1172/JCI137244

58. Pons S, Fodil S, Azoulay E, Zafrani L. The vascular endothelium: the cornerstone of organ dysfunction in severe SARS-CoV-2 infection. Crit Care. BioMed Central; 2020;24: 353–8. doi:10.1186/s13054-020-03062-7

59. Lowenstein CJ, Solomon SD. Severe COVID-19 is a Microvascular Disease. Circulation. Lippincott Williams & Wilkins Hagerstown, MD; 2020;191: 148. doi:10.1161/CIRCULATIONAHA.120.050354

60. Varga Z, Flammer AJ, Steiger P, Haberecker M, Andermatt R, Zinkernagel AS, et al. Endothelial cell infection and endotheliitis in COVID-19. The Lancet. Elsevier Ltd; 2020;395: 1417–1418. doi:10.1016/S0140-6736(20)30937-5

61. Amraei R, Rahimi N. COVID-19, Renin-Angiotensin System and Endothelial Dysfunction. Cells. Multidisciplinary Digital Publishing Institute; 2020;9: 1652. doi:10.3390/cells9071652

62. Teuwen L-A, Geldhof V, Pasut A, Carmeliet P. COVID-19: the vasculature unleashed. Nature Reviews Immunology. Nature Publishing Group; 2020;20: 389–391. doi:10.1038/s41577-020-0343-0

63. Gu SX, Tyagi T, Jain K, Gu VW, Lee SH, Hwa JM, et al. Thrombocytopathy and endotheliopathy: crucial contributors to COVID-19 thromboinflammation. Nat Rev Cardiol. Nature Publishing Group; 2021;18: 194–209. doi:10.1038/s41569-020-00469-1

64. Suvorava T, Kaesemeyer W. Targeting the Vascular Endothelium in the Treatment of COVID-19. J Cardiovasc Pharmacol. 2021;77: 1–3. doi:10.1097/FJC.0000000000000932

65. Bastard P, Rosen LB, Zhang Q, Michailidis E, Hoffmann H-H, Zhang Y, et al. Auto-antibodies against type I IFNs in patients with life-threatening COVID-19. Science. 2020;129: eabd4585. doi:10.1126/science.abd4585

66. Zhang Q, Bastard P, Liu Z, Le Pen J, Moncada-Velez M, Chen J, et al. Inborn errors of type I IFN immunity in patients with life-threatening COVID-19. Science. 2020;: eabd4570. doi:10.1126/science.abd4570

67. Park A, Iwasaki A. Type I and Type III Interferons - Induction, Signaling, Evasion, and Application to Combat COVID-19. Cell Host and Microbe. 2020;27: 870–878. doi:10.1016/j.chom.2020.05.008

68. Thorne LG, Bouhaddou M, Reuschl A-K, Zuliani-Alvarez L, Polacco B, Pelin A, et al. Evolution of enhanced innate immune evasion by the SARS-CoV-2 B.1.1.7 UK variant. bioRxiv. Cold Spring Harbor Laboratory; 2021;: 2021.06.06.446826. doi:10.1101/2021.06.06.446826

69. Sposito B, Broggi A, Pandolfi L, Crotta S, Clementi N, Ferrarese R, et al. The interferon landscape along the respiratory tract impacts the severity of COVID-19. Cell. 2021;184: 4953–4968.e16. doi:10.1016/j.cell.2021.08.016

70. Ziegler CGK, Miao VN, Owings AH, Navia AW, Tang Y, Bromley JD, et al. Impaired local intrinsic immunity to SARS-CoV-2 infection in severe COVID-19. Cell. 2021;184: 4713–4733.e22. doi:10.1016/j.cell.2021.07.023

71. Zhou Z, Ren L, Zhang L, Zhong J, Xiao Y, Jia Z, et al. Heightened Innate Immune Responses in the Respiratory Tract of COVID-19 Patients. Cell Host and Microbe. 2020;27: 883–890.e2. doi:10.1016/j.chom.2020.04.017

72. Hadjadj J, Yatim N, Barnabei L, Corneau A, Boussier J, Smith N, et al. Impaired type I interferon activity and inflammatory responses in severe COVID-19 patients. Science. 2020;369: 718–724. doi:10.1126/science.abc6027

73. Banerjee A, El-Sayes N, Budylowski P, Jacob RA, Richard D, Maan H, et al. Experimental and natural evidence of SARS-CoV-2-infection-induced activation of type I interferon responses. iScience. 2021;24: 102477. doi:10.1016/j.isci.2021.102477

74. Yuen C-K, Lam J-Y, Wong W-M, Mak L-F, Wang X, Chu H, et al. SARS-CoV-2 nsp13, nsp14, nsp15 and orf6 function as potent interferon antagonists. Emerging Microbes & Infections. Taylor & Francis; 2020;9: 1418–1428. doi:10.1080/22221751.2020.1780953

75. Miorin L, Kehrer T, Sanchez-Aparicio MT, Zhang K, Cohen P, Patel RS, et al. SARS-CoV-2 Orf6 hijacks Nup98 to block STAT nuclear import and antagonize interferon signaling. Proc Natl Acad Sci USA. 2020;5: 202016650–11. doi:10.1073/pnas.2016650117

76. Banerjee AK, Blanco MR, Bruce EA, Honson DD, Chen LM, Chow A, et al. SARS-CoV-2 disrupts splicing, translation, and protein trafficking to suppress host defenses. Cell. Elsevier Inc; 2020;: 1–66. doi:10.1016/j.cell.2020.10.004

77. Konno Y, Kimura I, Uriu K, Fukushi M, Irie T, Koyanagi Y, et al. SARS-CoV-2 ORF3b Is a Potent Interferon Antagonist Whose Activity Is Increased by a Naturally Occurring Elongation Variant. CellReports. 2020;32: 108185. doi:10.1016/j.celrep.2020.108185

78. Yin X, Riva L, Pu Y, Martin-Sancho L, Kanamune J, Yamamoto Y, et al. MDA5 Governs the Innate Immune Response to SARS-CoV-2 in Lung Epithelial Cells. CellReports. 2021;34: 108628. doi:10.1016/j.celrep.2020.108628

79. Lei X, Dong X, Ma R, Wang W, Xiao X, Tian Z, et al. Activation and evasion of type I interferon responses by SARS-CoV-2. Nature Communications. Nature Publishing Group; 2020;11: 3810–12. doi:10.1038/s41467-020-17665-9

80. Beyer DK, Forero A. Mechanisms of Antiviral Immune Evasion of SARS-CoV-2. J Mol Biol. 2021;: 167265. doi:10.1016/j.jmb.2021.167265

81. Xia H, Cao Z, Xie X, Zhang X, Chen JY-C, Wang H, et al. Evasion of Type I Interferon by SARS-CoV-2. CellReports. 2020;33: 108234. doi:10.1016/j.celrep.2020.108234

82. Suryawanshi RK, Koganti R, Agelidis A, Patil CD, Shukla D. Dysregulation of Cell Signaling by SARS-CoV-2. Trends in Microbiology. 2021;29: 224–237. doi:10.1016/j.tim.2020.12.007

83. Wickenhagen A, Sugrue E, Lytras S, Kuchi S, Noerenberg M, Turnbull ML, et al. A prenylated dsRNA sensor protects against severe COVID-19. Science. American Association for the Advancement of Science; 2021;: eabj3624. doi:10.1126/science.abj3624

84. Hsu JC-C, Laurent-Rolle M, Pawlak JB, Wilen CB, Cresswell P. Translational shutdown and evasion of the innate immune response by SARS-CoV-2 NSP14 protein. Proc Natl Acad Sci USA. National Academy of Sciences; 2021;118. doi:10.1073/pnas.2101161118

85. Zhao Y, Sui L, Wu P, Wang W, Wang Z, Yu Y, et al. A dual-role of SARS-CoV-2 nucleocapsid protein in regulating innate immune response. Signal Transduct Target Ther. Nature Publishing Group; 2021;6: 331–14. doi:10.1038/s41392-021-00742-w

86. Sola I, Galán C, Mateos-Gómez PA, Palacio L, Zuñiga S, Cruz JL, et al. The polypyrimidine tract-binding protein affects coronavirus RNA accumulation levels and relocalizes viral RNAs to novel cytoplasmic domains different from replication-transcription sites. J Virol. 3rd ed. 2011;85: 5136–5149. doi:10.1128/JVI.00195-11

87. Raaben M, Groot Koerkamp MJA, Rottier PJM, de Haan CAM. Mouse hepatitis coronavirus replication induces host translational shutoff and mRNA decay, with concomitant formation of stress granules and processing bodies. Cellular Microbiology. 2007;9: 2218–2229. doi:10.1111/j.1462-5822.2007.00951.x

88. Ackermann M, Mentzer SJ, Kolb M, Jonigk D. Inflammation and Intussusceptive Angiogenesis in COVID-19: everything in and out of Flow. Eur Respir J. 2020;383: 2003147. doi:10.1183/13993003.03147-2020

89. Nascimento Conde J, Schutt WR, Gorbunova EE, Mackow ER. Recombinant ACE2 Expression Is Required for SARS-CoV-2 To Infect Primary Human Endothelial Cells and Induce Inflammatory and Procoagulative Responses. Patton JT, editor. mBio. American Society for Microbiology; 2020;11. doi:10.1128/mBio.03185-20

90. Castle EL, Robinson C-A, Douglas P, Rinker KD, Corcoran JA. Viral manipulation of a mechanoresponsive signaling axis disassembles processing bodies. Mol Cell Biol. 2021;: MCB0039921. doi:10.1128/MCB.00399-21

91. Sola I, Almazán F, Zuñiga S, Enjuanes L. Continuous and Discontinuous RNA Synthesis in Coronaviruses. Annu Rev Virol. Annual Reviews; 2015;2: 265–288. doi:10.1146/annurev-virology-100114-055218

92. Ayache J, Bénard M, Ernoult-Lange M, Minshall N, Standart N, Kress M, et al. P-body assembly requires DDX6 repression complexes rather than decay or Ataxin2/2L complexes. Matera AG, editor. Mol Biol Cell. The American Society for Cell Biology; 2015;26: 2579–2595. doi:10.1091/mbc.E15-03-0136

93. Gordon DE, Jang GM, Bouhaddou M, Xu J, Obernier K, White KM, et al. A SARS-CoV-2 protein interaction map reveals targets for drug repurposing. Nature. Nature Publishing Group; 2020;583: 459–468. doi:10.1038/s41586-020-2286-9

94. Min Y-Q, Mo Q, Wang J, Deng F, Wang H, Ning Y-J. SARS-CoV-2 nsp1: Bioinformatics, Potential Structural and Functional Features, and Implications for Drug/Vaccine Designs. Front Microbiol. Frontiers; 2020;11: 587317. doi:10.3389/fmicb.2020.587317

95. Zeng W, Liu G, Ma H, Zhao D, Yang Y, Liu M, et al. Biochemical characterization of SARS-CoV-2 nucleocapsid protein. Biochem Biophys Res Commun. 2020;527: 618–623. doi:10.1016/j.bbrc.2020.04.136

96. Bai Z, Cao Y, Liu W, Li J. The SARS-CoV-2 Nucleocapsid Protein and Its Role in Viral Structure, Biological Functions, and a Potential Target for Drug or Vaccine Mitigation. Viruses. Multidisciplinary Digital Publishing Institute; 2021;13: 1115. doi:10.3390/v13061115

97. Peng T-Y, Lee K-R, Tarn W-Y. Phosphorylation of the arginine/serine dipeptide-rich motif of the severe acute respiratory syndrome coronavirus nucleocapsid protein modulates its multimerization, translation inhibitory activity and cellular localization. FEBS J. John Wiley & Sons, Ltd; 2008;275: 4152–4163. doi:10.1111/j.1742-4658.2008.06564.x

98. McBride R, van Zyl M, Fielding BC. The coronavirus nucleocapsid is a multifunctional protein. Viruses. Multidisciplinary Digital Publishing Institute; 2014;6: 2991–3018. doi:10.3390/v6082991

99. Cong Y, Ulasli M, Schepers H, Mauthe M, V'kovski P, Kriegenburg F, et al. Nucleocapsid Protein Recruitment to Replication-Transcription Complexes Plays a Crucial Role in Coronaviral Life Cycle. Dutch RE, editor. J Virol. American Society for Microbiology Journals; 2020;94: 181. doi:10.1128/JVI.01925-19

100. Lu S, Ye Q, Singh D, Villa E, Cleveland DW, Corbett KD. The SARS-CoV-2 Nucleocapsid phosphoprotein forms mutually exclusive condensates with RNA and the membrane-associated M protein. bioRxiv. 2020;18: 479. doi:10.1101/2020.07.30.228023

101. Cascarina SM, Ross ED. A proposed role for the SARS-CoV-2 nucleocapsid protein in the formation and regulation of biomolecular condensates. FASEB j. 2020;34: 9832–9842. doi:10.1096/fj.202001351

102. Chen H, Cui Y, Han X, Hu W, Sun M, Zhang Y, et al. Liquid-liquid phase separation by SARS-CoV-2 nucleocapsid protein and RNA. Cell Res. Nature Publishing Group; 2020;30: 1143–1145. doi:10.1038/s41422-020-00408-2

103. Savastano A, Ibáñez de Opakua A, Rankovic M, Zweckstetter M. Nucleocapsid protein of SARS-CoV-2 phase separates into RNA-rich polymerase-containing condensates.

Nature Communications. Nature Publishing Group; 2020;11: 6041–10. doi:10.1038/s41467-020-19843-1

104. Iserman C, Roden CA, Boerneke MA, Sealfon RSG, McLaughlin GA, Jungreis I, et al. Genomic RNA Elements Drive Phase Separation of the SARS-CoV-2 Nucleocapsid. Mol Cell. 2020;80: 1078–1091.e6. doi:10.1016/j.molcel.2020.11.041

105. Carlson CR, Asfaha JB, Ghent CM, Howard CJ, Hartooni N, Safari M, et al. Phosphoregulation of Phase Separation by the SARS-CoV-2 N Protein Suggests a Biophysical Basis for its Dual Functions. Mol Cell. 2020;80: 1092–1103.e4. doi:10.1016/j.molcel.2020.11.025

106. Cubuk J, Alston JJ, Incicco JJ, Singh S, Stuchell-Brereton MD, Ward MD, et al. The SARS-CoV-2 nucleocapsid protein is dynamic, disordered, and phase separates with RNA. Nature Communications. Nature Publishing Group; 2021;12: 1936–17. doi:10.1038/s41467-021-21953-3

107. Sa Ribero M, Jouvenet N, Dreux M, Nisole S. Interplay between SARS-CoV-2 and the type I interferon response. PLoS Pathogens. Public Library of Science; 2020;16: e1008737. doi:10.1371/journal.ppat.1008737

108. Gori Savellini G, Anichini G, Gandolfo C, Cusi MG. SARS-CoV-2 N Protein Targets TRIM25-Mediated RIG-I Activation to Suppress Innate Immunity. Viruses. Multidisciplinary Digital Publishing Institute; 2021;13: 1439. doi:10.3390/v13081439

109. Oliveira SC, de Magalhães MTQ, Homan EJ. Immunoinformatic Analysis of SARS-CoV-2 Nucleocapsid Protein and Identification of COVID-19 Vaccine Targets. Front Immunol. Frontiers; 2020;11: 587615. doi:10.3389/fimmu.2020.587615

110. Parker MD, Lindsey BB, Leary S, Gaudieri S, Chopra A, Wyles M, et al. Subgenomic RNA identification in SARS-CoV-2 genomic sequencing data. Genome Res. Cold Spring Harbor Lab; 2021;31: 645–658. doi:10.1101/gr.268110.120

111. Leary S, Gaudieri S, Parker MD, Chopra A, James I, Pakala S, et al. Generation of a Novel SARS-CoV-2 Sub-genomic RNA Due to the R203K/G204R Variant in Nucleocapsid: Homologous Recombination has Potential to Change SARS-CoV-2 at Both Protein and RNA Level. Pathog Immun. 2021;6: 27–49. doi:10.20411/pai.v6i2.460

112. Saffran HA, Pare JM, Corcoran JA, Weller SK, Smiley JR. Herpes simplex virus eliminates host mitochondrial DNA. EMBO Rep. 2007;8: 188–193. doi:10.1038/sj.embor.7400878

113. Corcoran JA, Saffran HA, Duguay BA, Smiley JR. Herpes simplex virus UL12.5 targets mitochondria through a mitochondrial localization sequence proximal to the N terminus. J Virol. 2009;83: 2601–2610. doi:10.1128/JVI.02087-08

114. Gordon DE, Hiatt J, Bouhaddou M, Rezelj VV, Ulferts S, Braberg H, et al. Comparative host-coronavirus protein interaction networks reveal pan-viral disease mechanisms. Science. 2020;11: eabe9403–38. doi:10.1126/science.abe9403

115. Nabeel-Shah S, Lee H, Ahmed N, Marcon E, Farhangmehr S, Pu S, et al. SARS-CoV-2 Nucleocapsid protein attenuates stress granule formation and alters gene expression via direct interaction with host mRNAs. bioRxiv. Cold Spring Harbor Laboratory; 2020;: 2020.10.23.342113. doi:10.1101/2020.10.23.342113

116. Luo L, Li Z, Zhao T, Ju X, Ma P, Jin B, et al. SARS-CoV-2 nucleocapsid protein phase separates with G3BPs to disassemble stress granules and facilitate viral production. Sci Bull (Beijing). 2021;66: 1194–1204. doi:10.1016/j.scib.2021.01.013

117. Zheng Z-Q, Wang S-Y, Xu Z-S, Fu Y-Z, Wang Y-Y. SARS-CoV-2 nucleocapsid protein impairs stress granule formation to promote viral replication. Cell Discov. Nature Publishing Group; 2021;7: 38–11. doi:10.1038/s41421-021-00275-0

118. Wang J, Shi C, Xu Q, Yin H. SARS-CoV-2 nucleocapsid protein undergoes liquid-liquid phase separation into stress granules through its N-terminal intrinsically disordered region. Cell Discov. Nature Publishing Group; 2021;7: 5–5. doi:10.1038/s41421-020-00240-3

119. Dougherty JD, Reineke LC, Lloyd RE. mRNA decapping enzyme 1a (Dcp1a)-induced translational arrest through protein kinase R (PKR) activation requires the N-terminal enabled vasodilator-stimulated protein homology 1 (EVH1) domain. J Biol Chem. 2014;289: 3936–3949. doi:10.1074/jbc.M113.518191

120. Schmidt N, Lareau CA, Keshishian H, Ganskih S, Schneider C, Hennig T, et al. The SARS-CoV-2 RNA-protein interactome in infected human cells. Nat Microbiol. Nature Publishing Group; 2021;6: 339–353. doi:10.1038/s41564-020-00846-z

121. Tibble RW, Depaix A, Kowalska J, Jemielity J, Gross JD. Biomolecular condensates amplify mRNA decapping by coupling protein interactions with conformational changes in Dcp1/Dcp2. 2020;60th Anniversary: 600–36. doi:10.1101/2020.07.09.195057

122. Tenekeci U, Poppe M, Beuerlein K, Buro C, Müller H, Weiser H, et al. K63-Ubiquitylation and TRAF6 Pathways Regulate Mammalian P-Body Formation and mRNA Decapping. Mol Cell. 2016;62: 943–957. doi:10.1016/j.molcel.2016.05.017

123. Li Y, Chen R, Zhou Q, Xu Z, Li C, Wang S, et al. LSm14A is a processing body-associated sensor of viral nucleic acids that initiates cellular antiviral response in the early phase of viral infection. Proc Natl Acad Sci USA. 2012;109: 11770–11775. doi:10.1073/pnas.1203405109

124. Rzeczkowski K, Beuerlein K, Müller H, Dittrich-Breiholz O, Schneider H, Kettner-Buhrow D, et al. c-Jun N-terminal kinase phosphorylates DCP1a to control formation of P bodies. J Cell Biol. 2011;194: 581–596. doi:10.1083/jcb.201006089

125. Stoecklin G, Mayo T, Anderson P. ARE-mRNA degradation requires the 5“-3” decay pathway. EMBO Rep. 2006;7: 72–77. doi:10.1038/sj.embor.7400572

126. Banerjee A, Nasir JA, Budylowski P, Yip L, Aftanas P, Christie N, et al. Isolation, Sequence, Infectivity, and Replication Kinetics of Severe Acute Respiratory Syndrome Coronavirus 2. Emerging Infect Dis. 2020;26: 2054–2063. doi:10.3201/eid2609.201495

127. Mendoza EJ, Manguiat K, Wood H, Drebot M. Two Detailed Plaque Assay Protocols for the Quantification of Infectious SARS-CoV-2. Curr Protoc Microbiol. John Wiley & Sons, Ltd; 2020;57: cpmc105. doi:10.1002/cpmc.105

128. Kamentsky L, Jones TR, Fraser A, Bray M-A, Logan DJ, Madden KL, et al. Improved structure, function and compatibility for CellProfiler: modular high-throughput image analysis software. Bioinformatics. 2011;27: 1179–1180. doi:10.1093/bioinformatics/btr095

129. Johnston BP, Pringle ES, McCormick C. KSHV activates unfolded protein response sensors but suppresses downstream transcriptional responses to support lytic replication. Swaminathan S, editor. PLoS Pathogens. 2019;15: e1008185. doi:10.1371/journal.ppat.1008185

A

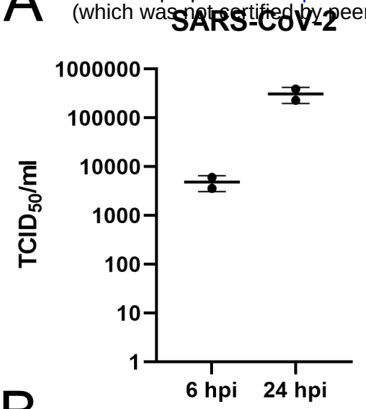

B

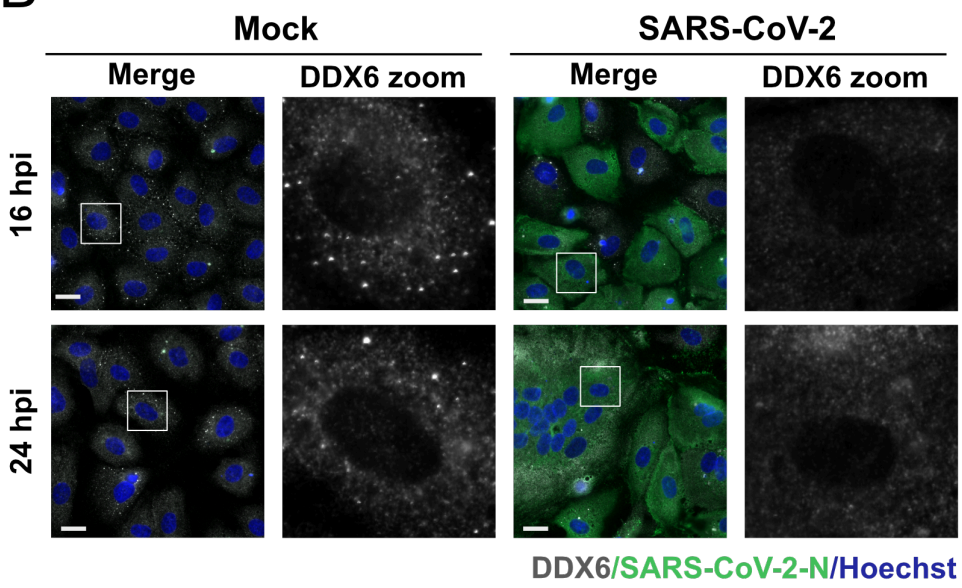

C

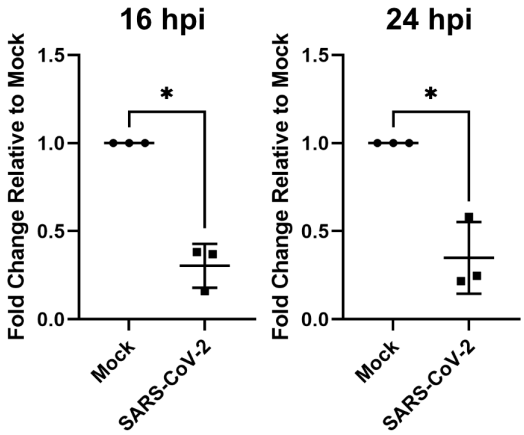

D

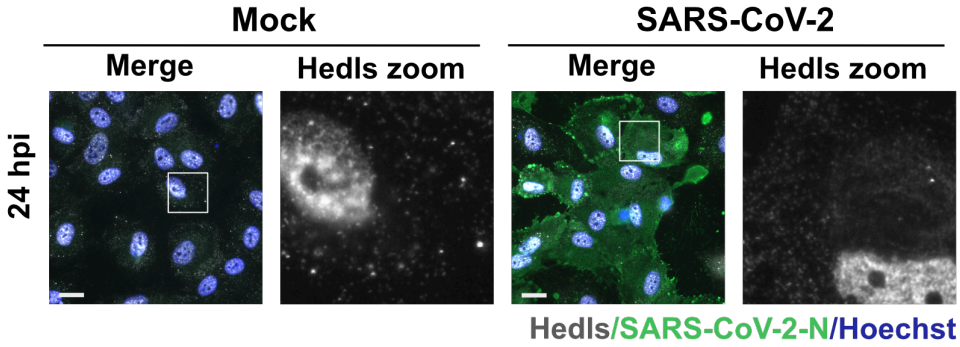

E

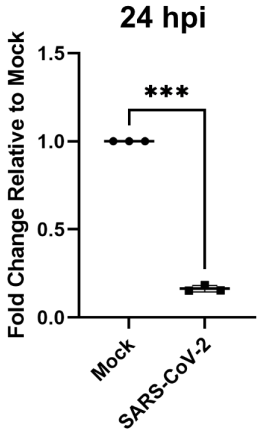

F

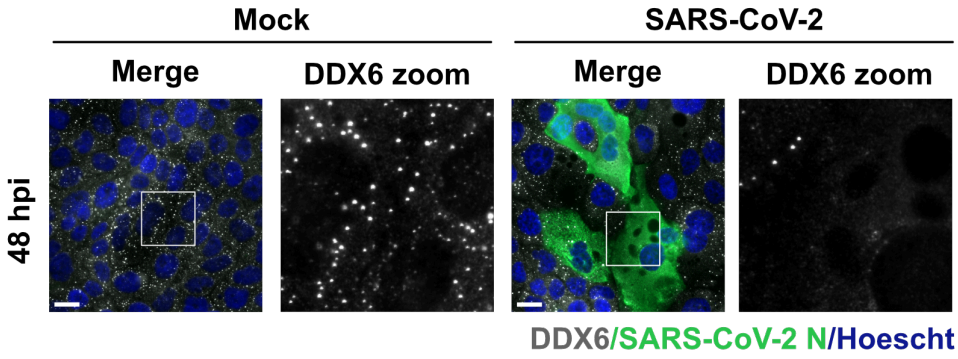

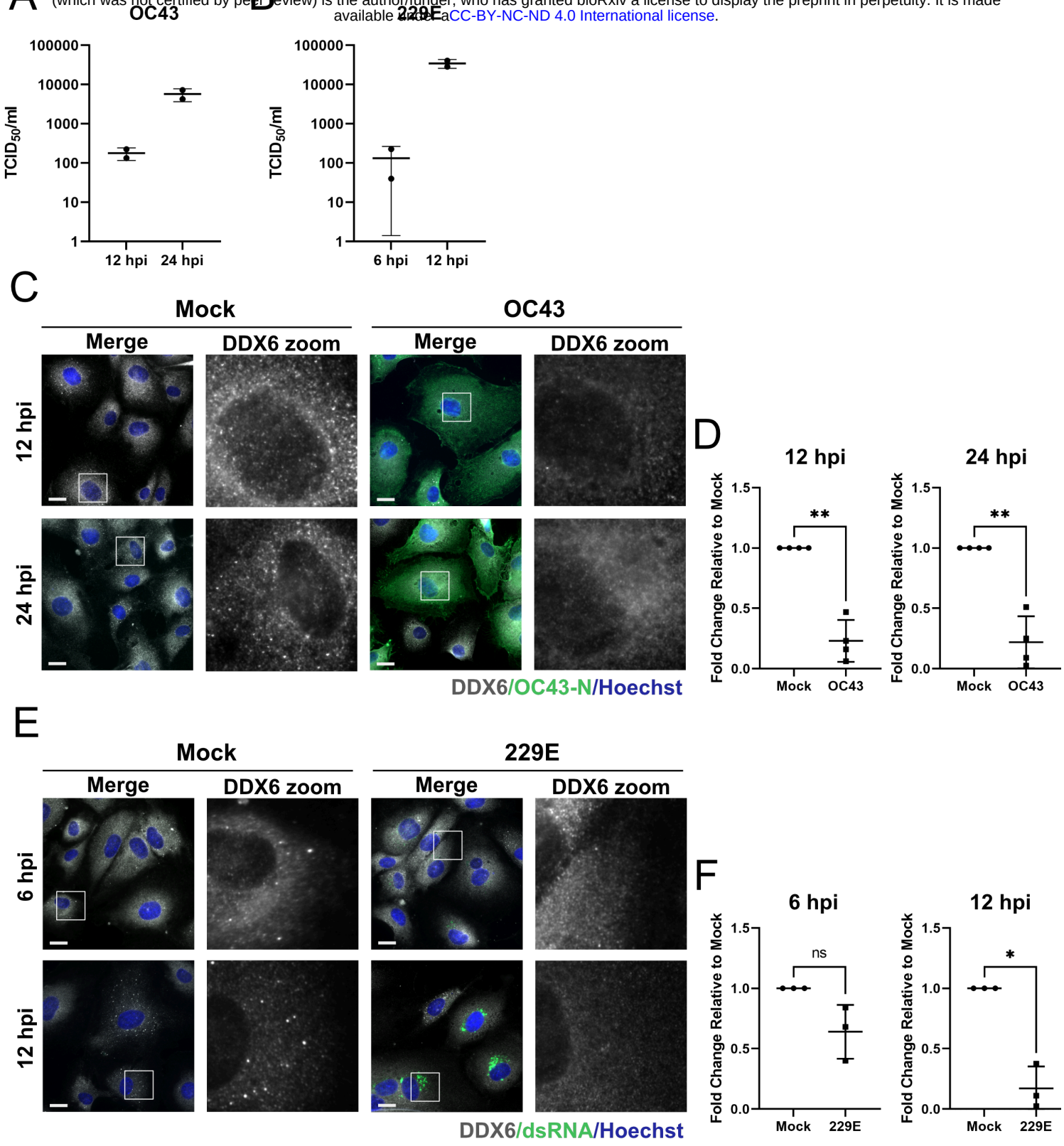

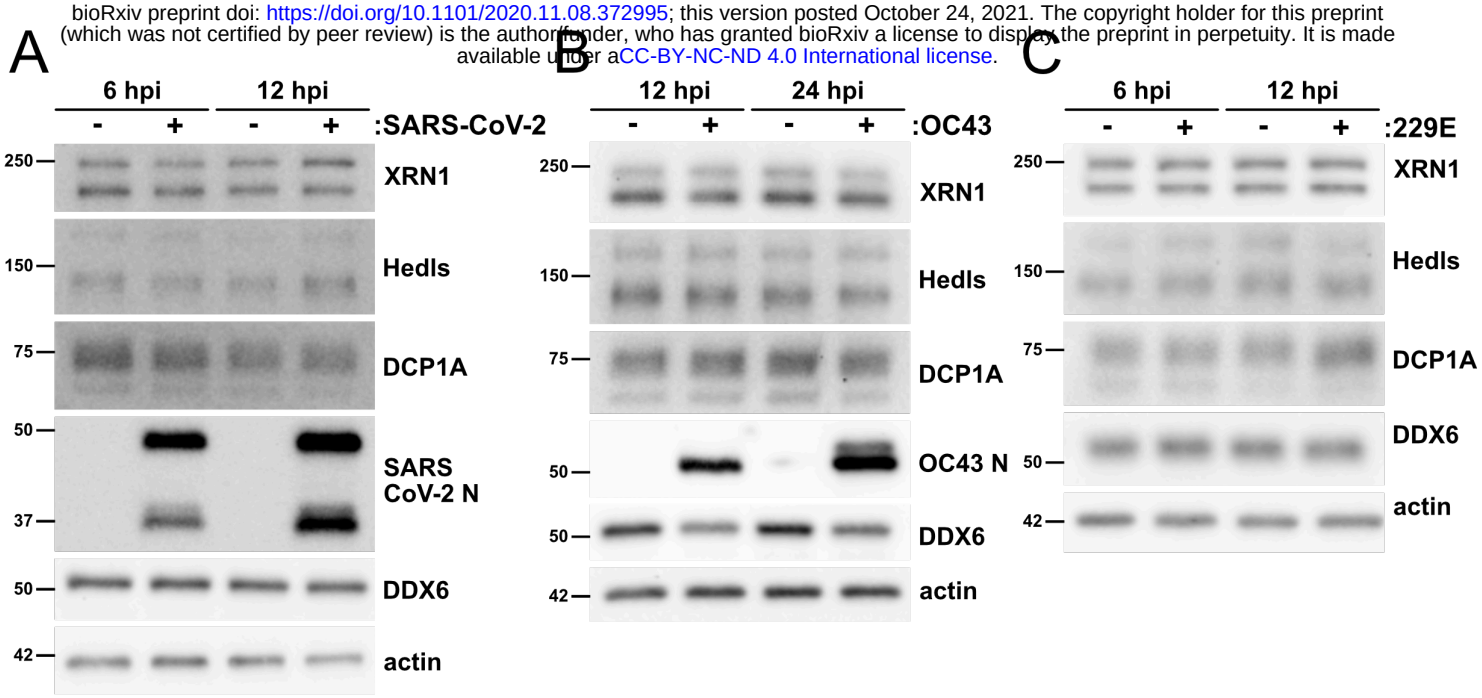

A

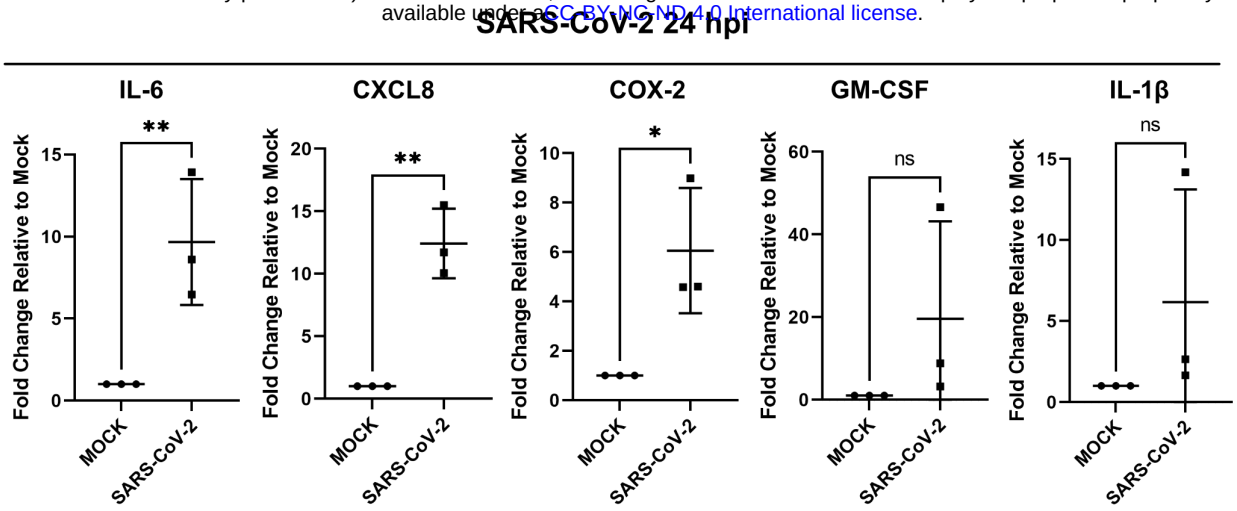

B

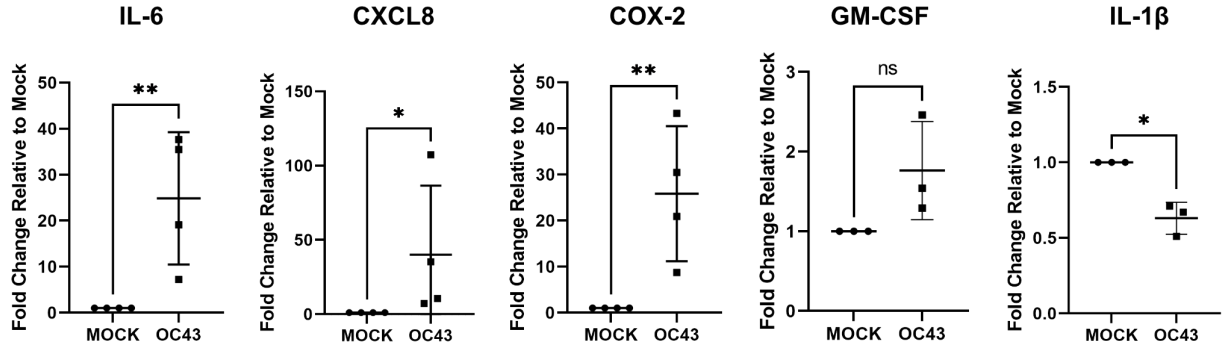

C

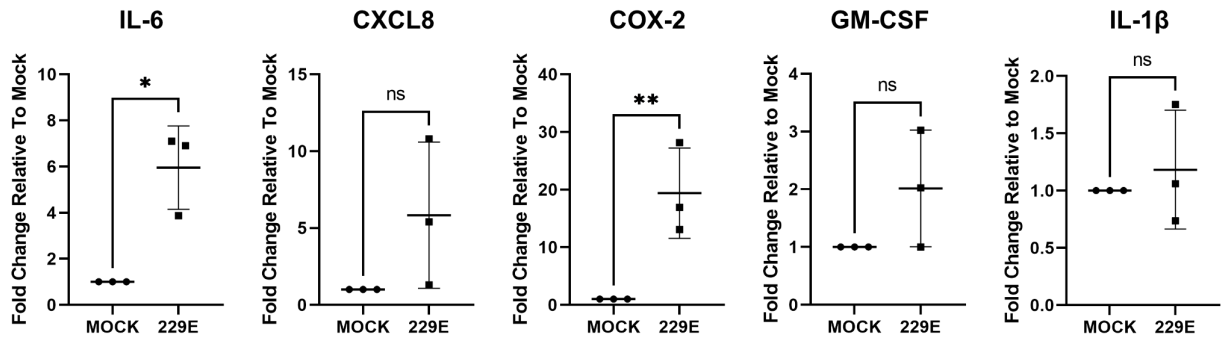

A

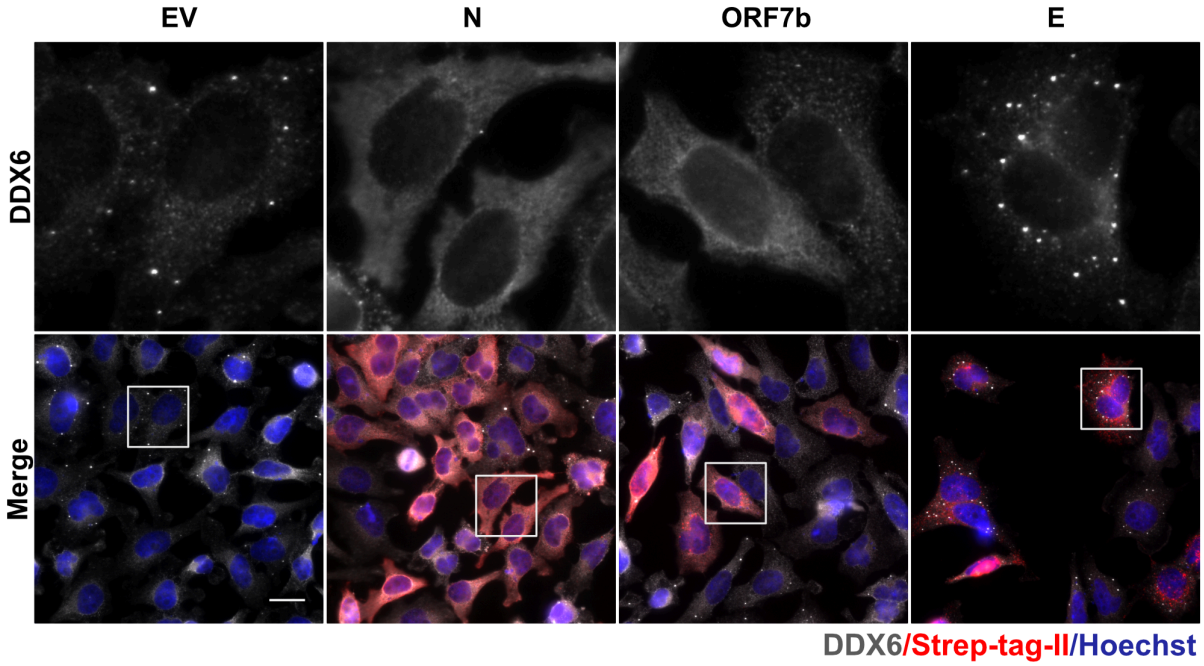

B

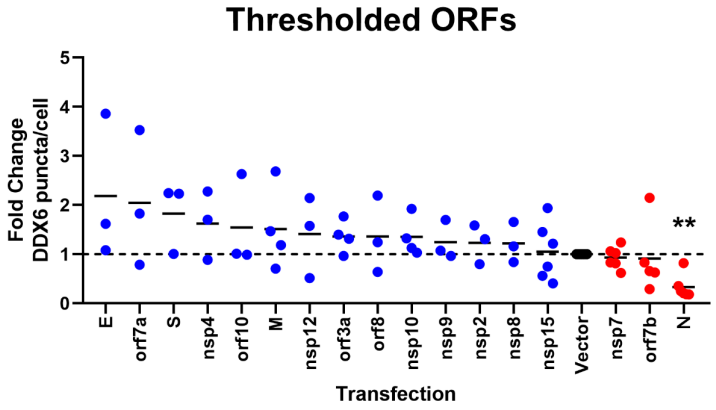

C

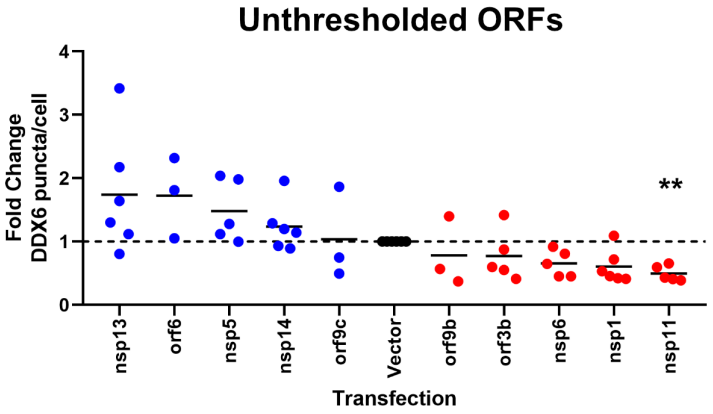

D

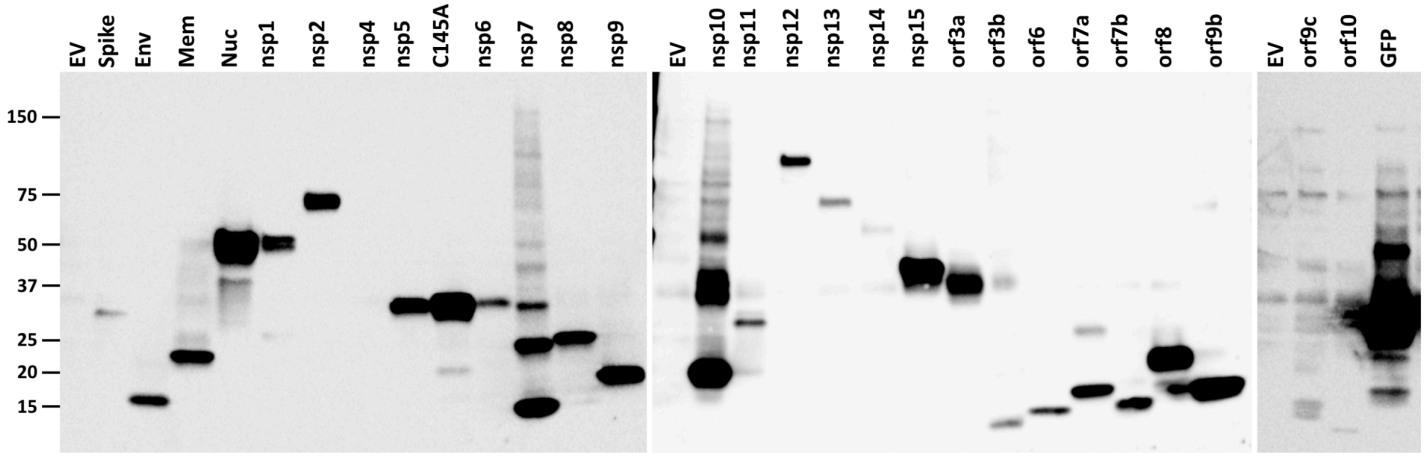

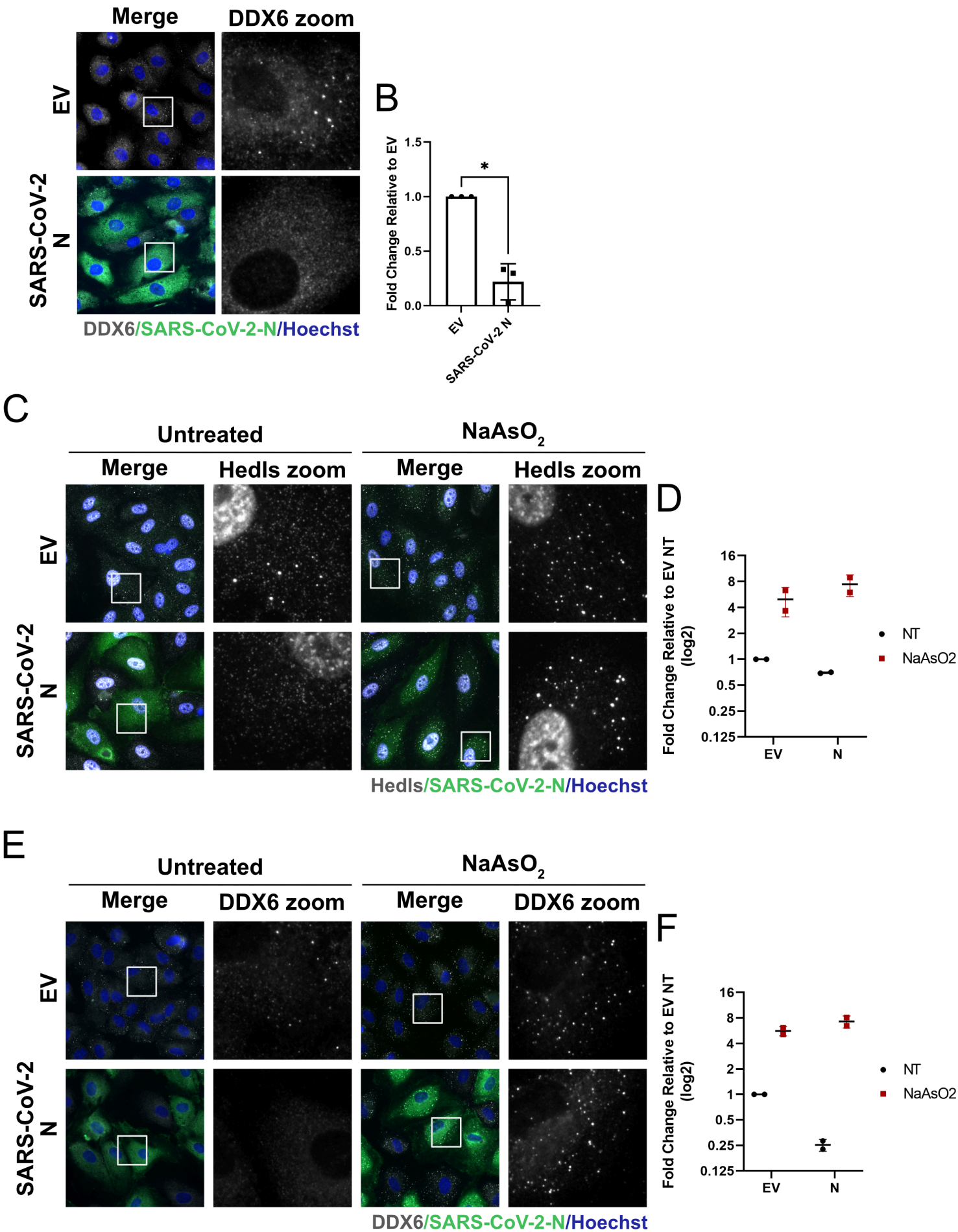

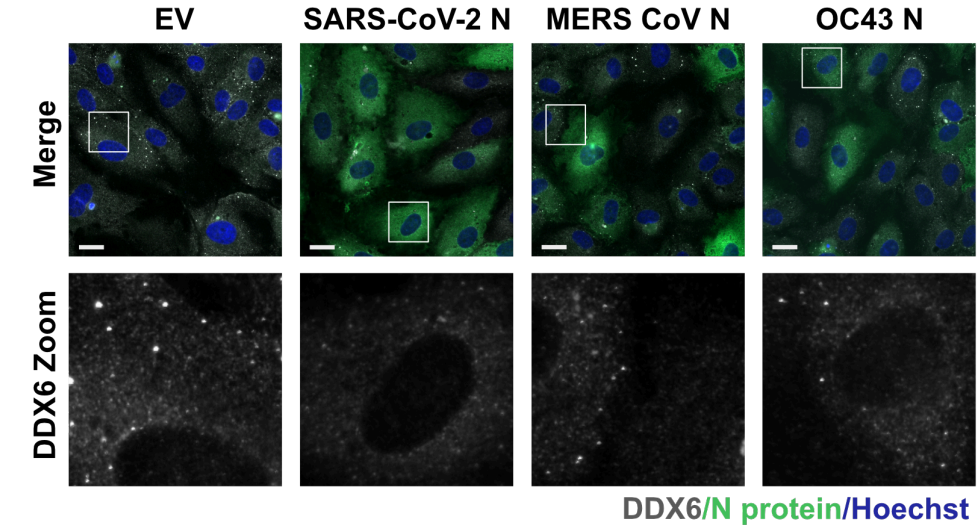

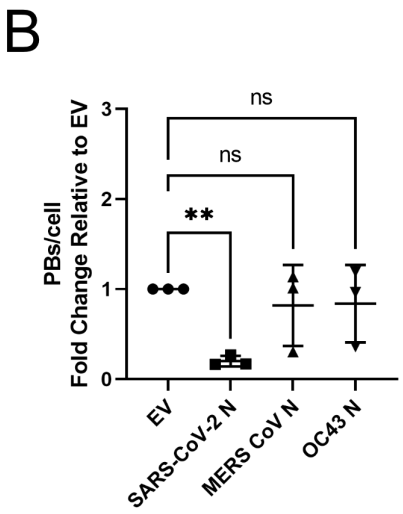

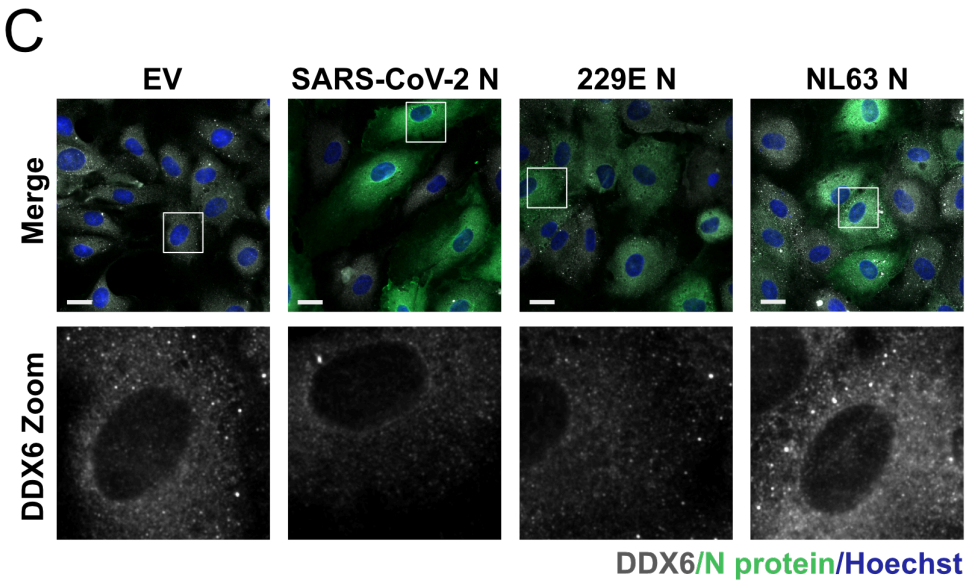

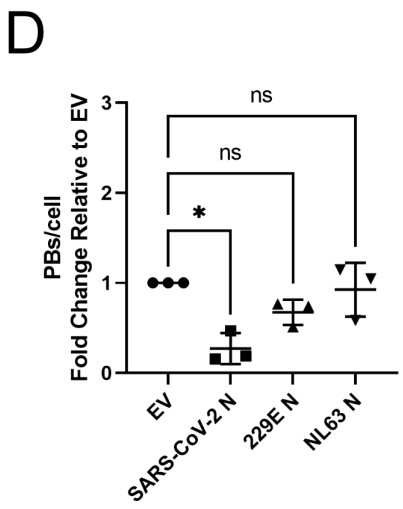

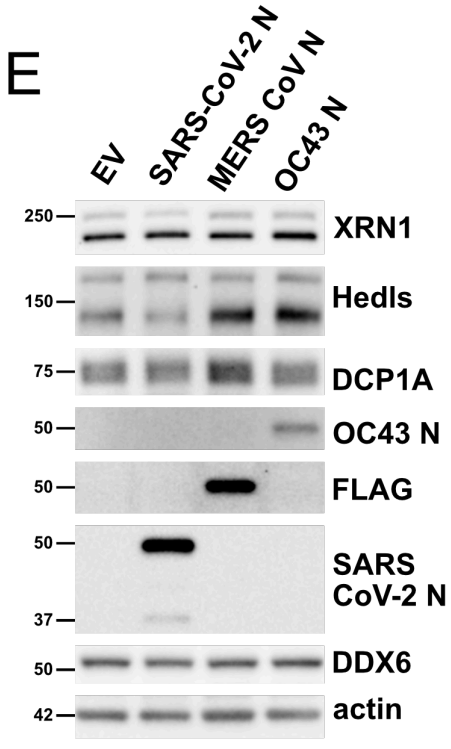

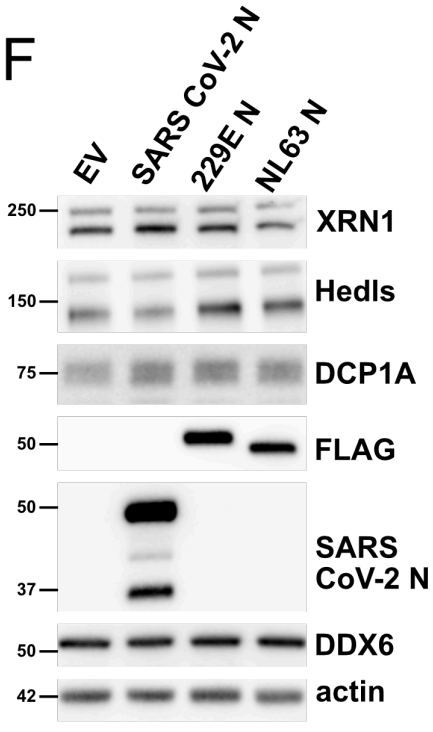

A

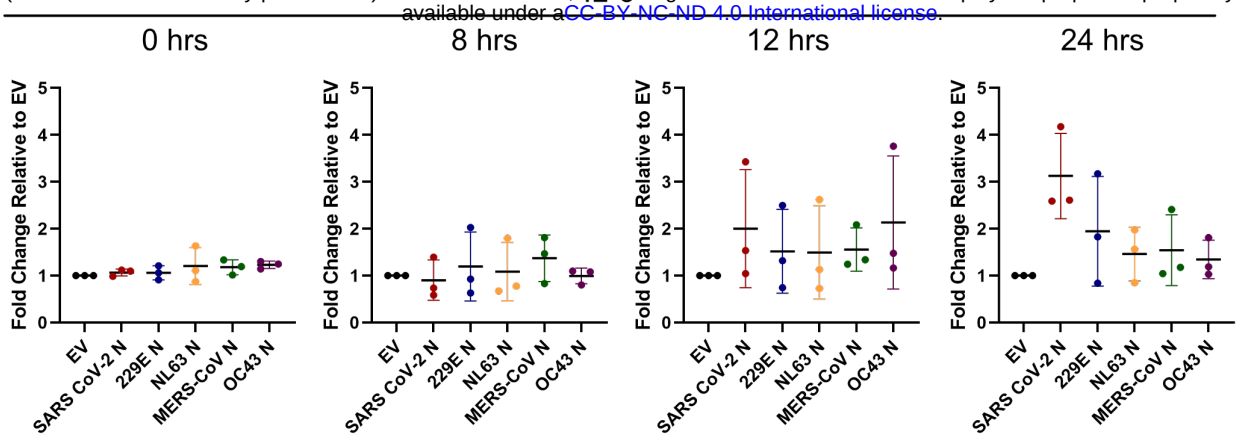

B

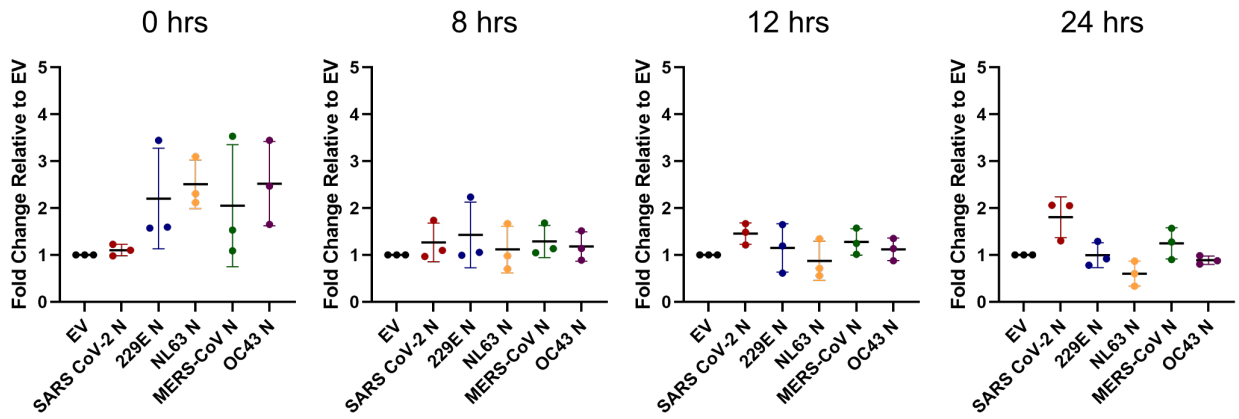

C

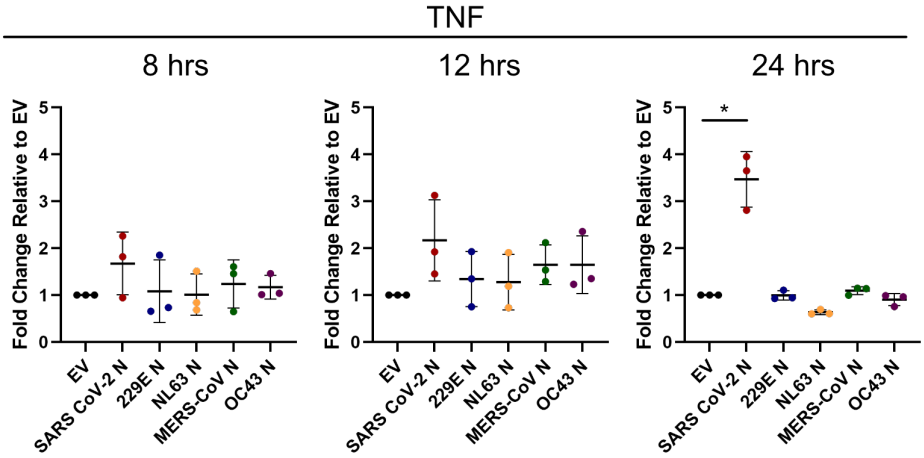

A

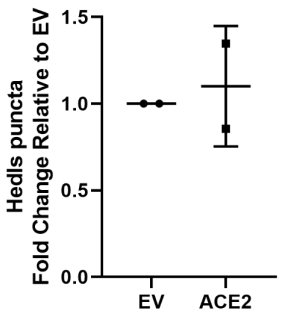

B

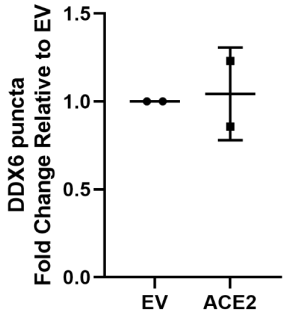

A

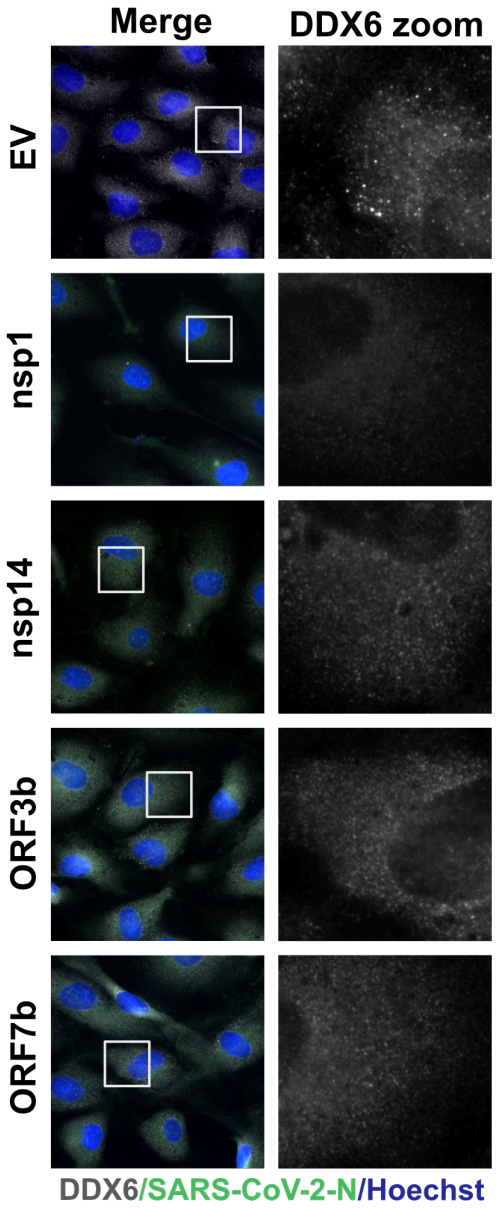

B

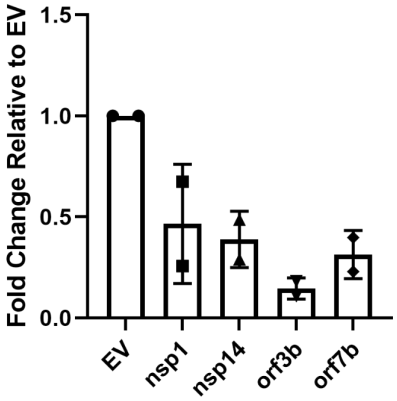

C